Mathematical Medicine and Biology (2017) **00**, 1–00
doi: 10.1093/imammb/dqx001

A Two-phase mixture model of platelet aggregation

JIAN DU[†]
Department of Mathematical Sciences, Florida Institute of Technology, Melbourne, Florida 32901, USA
[†]Corresponding author. Email: jdu@fit.edu

AND

AARON L. FOGELSON
Departments of Mathematics and Bioengineering, University of Utah, Salt Lake City, UT 84112, USA

[Received on 20 August 2016; revised on 30 December 2016; accepted on 4 January 2017]

We present a two-phase model of platelet aggregation in coronary-artery-sized blood vessels. The model tracks the number densities of three platelet populations as well as the concentration of a platelet activating chemical. Through the formation of elastic bonds, activated platelets can cohere with one another to form a platelet thrombus. Bound platelets in a thrombus move in a velocity field different from that of the bulk fluid. Stresses produced by the elastic bonds act on the bound platelet material. Movement of the bound platelet material and that of the background fluid are coupled through an interphase drag and an incompressibility constraint. The relative motion between bound platelets and the background fluid permits intraclot transport of individual platelets and activating chemical, allows the bound platelet density to reach levels much higher than the platelet density in the bulk blood, and allows thrombus formation to occur on a physiological timescale, all of which were precluded by our earlier single phase model. Computational results from the two-phase model indicate that through complicated fluid-structure interactions, the platelet thrombus can develop significant spatial inhomogeneities and that the amount of intraclot flow may greatly affect the growth, density, and stability of a thrombus.

Keywords: thrombosis; continuum model; viscoelastic; porous medium.

1. Introduction

Most heart attacks are triggered by the occlusion of a coronary artery by a platelet-rich blood clot or thrombus that forms after an atherosclerotic plaque in that artery ruptures. Plaques form slowly and gradually produce a stenosis (constriction) of the vessel lumen which changes the local flow. While development of the plaque likely takes place over a period of many years, the formation of an occlusive thrombus on the plaque after it ruptures can occur in minutes and can be the proximal cause of stopping the flow of oxygen-rich blood to portions of the heart.

Plaque rupture exposes to the blood a number of strongly clot-promoting materials to which circulating platelets can adhere and which stimulate the platelets to undergo a multifaceted activation process. Adhesion of platelets to the plaque is accomplished through the formation of molecular bonds between receptors on the platelets' surfaces and specific proteins embedded in the plaque (platelet GPIbα receptors bind to von Willebrand factor; platelet GPVI and $\alpha_2\beta_1$ receptors bind to collagen). Activation of a platelet induces activation of a large number of an additional type of platelet surface receptor (integrin $\alpha_{IIb}\beta_3$ receptors) which can serve as anchors for fibrinogen- and von Willebrand factor-mediated molecular bonds between that platelet and other activated platelets. Activation of a platelet also causes it to release

into the surrounding fluid soluble agonists (in particular, adenosine diphosphate and thromboxane A_2) which can activate other platelets. These processes are reviewed in Fogelson & Neeves (2015). A second process called coagulation is also initiated by material exposed by plaque rupture. It consists of tightly regulated enzymatic reactions, many of which take place on the accumulating platelets' surfaces, that lead to production of the critical enzyme thrombin on the platelets. Thrombin released into the plasma activates additional platelets and it also converts the soluble plasma protein fibrinogen into fibrin monomers which spontaneously polymerize to form a gel around the accumulated platelets. The coagulation reactions and fibrin polymerization are not treated in the model described in this article. For modelling of those aspects of clot formation, see Kuharsky & Fogelson 2001; Fogelson & Tania 2005; Guy & Fogelson 2007; Fogelson & Keener 2010; Leiderman & Fogelson 2011; Fogelson *et al.* 2012; Leiderman & Fogelson 2013. For a review of clot formation and the influence of fluid dynamics on it, see Fogelson & Neeves (2015).

The coronary arteries in which these events occur have diameters on the scale of millimetres, a plaque may have a length on the scale of centimetres, and a typical platelet count or number density is 250,000/μl, so many millions of platelets may interact with the plaque at each time instant. Hence, it is not reasonable to study thrombosis on a ruptured plaque using models that track the motion and behaviour of discrete platelets (Fogelson, 1984; Fogelson & Guy 2008; Xu *et al.* 2008; Flamm & Diamond 2012). Instead, we developed and studied a continuum model of platelet thrombus formation in a moving fluid in response to plaque rupture (Fogelson 1992, 1993; Wang & Fogelson 1999; Fogelson & Guy, 2004; Fogelson & Guy 2008). The successes and limitations of that model are the motivation for the current paper. We refer to the older model as our 'single-phase' platelet continuum model to distinguish it from the two-phase continuum model that is the subject of this article.

Other models that treat platelets in a continuum fashion have been proposed. Some treat the edge of the growing thrombus as a moving boundary and ignore the mechanics of the thrombus itself (Weller 2010; Tokarev *et al.* 2012; Storti *et al.* 2014). The thrombus has also been treated as an irreversibly growing impermeable Hookean elastic solid in contact with the fluid (Storti & Van De Vosse 2014). Single phase viscoelastic models of clot development have also been proposed (Anand *et al.* 2005).

Our single-phase platelet continuum model was derived beginning with a two-scale view of platelet thrombus formation in a coronary-artery-size vessel. The two scales are the macro- or millimetre scale of the vessel and the micro- or micron scale of the platelet. The single-phase model tracks the number densities of two populations of platelets, unactivated and activated, as they move and interact with one another and with an injured region on the vessel wall. In the model, unactivated platelets can become activated ones if they encounter a sufficiently high concentration of an activating chemical released by other platelets, or if they come into close proximity of reactive sites on the injury. The model tracks the release, motion and degradation of the activating chemical. It also includes the formation and breaking of elastic bonds between activated platelets or between activated platelets and the injury, and it is the ability of these bonds to sustain forces that gives a thrombus its mechanical coherence. The distribution of bonds in the two-scale model is tracked through an elastic bond function E. The fluid velocity, the platelet number densities and the activating chemical concentration are all regarded as functions of the macroscale spatial variable and time.

In contrast, the elastic bond function E, which describes the bonds between activated platelets at macroscale location $\mathbf{x}$ and those within a region around $\mathbf{x}$ of radius a few platelet diameters is taken to be a function of both the macro- and micro-scale spatial variables. That is, $E = E(\mathbf{x}, \epsilon^{-1}\mathbf{r}, t) = E(\mathbf{x}, \mathbf{y}, t)$ and $E(\mathbf{x}, \epsilon^{-1}\mathbf{r}, t)d\mathbf{x}d\mathbf{r}$ give the number of elastic bonds between activated platelets in small volumes centred at locations $\mathbf{x}$ and $\mathbf{r}$. Here, ϵ is the ratio of platelet and vessel scale lengths and is a small parameter. We derived an evolution equation for E (to leading order in ϵ) that involves advection at the

ambient fluid velocity and redistribution of bond lengths and orientations because of the difference in the velocity at the two ends of a bond. In the two-scale formulation of the model, the bond formation rate, the bond breaking rate and the individual bond elastic stiffness can all be arbitrary specified functions of the (scaled) interplatelet distance $|\mathbf{y}|$. The bonds affect the fluid mechanics because they produce a 'platelet stress' $\underline{\underline{\sigma}}^{\mathrm{p}}(\mathbf{x},t) = \frac{1}{2}\int_{\mathbf{y}} E(\mathbf{x},\mathbf{y},t)S(|\mathbf{y}|)\mathbf{y}\mathbf{y}^T d\mathbf{y}$, where $S(|\mathbf{y}|)$ is the bond stiffness function, whose divergence appears in the fluid dynamics equations. All species in the model, the fluid, platelets and activating chemical, as well as the interplatelet bonds, and therefore the stresses they generate, move in the velocity field determined by these fluid dynamics equations.

In Wang & Fogelson (1999), we formulated a computational method for studying the two-scale version of the single-phase model. For most of our studies of the model, however, we use a form in which the micro-scale variable $\mathbf{y}$ does not appear. Instead, an evolution equation for the bond stress tensor $\underline{\underline{\sigma}}^{\mathrm{p}}(\mathbf{x},t)$ defined above is used. Under the assumption that individual platelet-platelet bonds break at a constant rate and behave as Hookean springs with zero rest length, an exact evolution equation for $\underline{\underline{\sigma}}^{\mathrm{p}}$ can be derived (Fogelson 1992). For the more realistic case that bonds break at a rate that varies with their length (i.e. with the strain on them), an approximate closure form of the stress evolution equation was derived in Fogelson & Guy (2008). In it, the breaking rate is a function of the root mean squared bond length for activated platelets at $\mathbf{x}$. As shown in the Appendix, this quantity can be computed from macroscale quantities without reference to the microscale.

We used the single phase model to begin to study thrombus formation on a ruptured atherosclerotic plaque. The vessel geometry, including that of the plaque, was specified and a portion of the plaque was designated as 'ruptured'. Thrombus formation began when platelets were activated by and formed bonds with reactive sites in the injured portion of the plaque. The thrombus grew because of the release and spread of activating chemical which in turn led to further platelet activation and stress development due to platelet-platelet bond formation. The model displayed many of the behaviours observed (or thought to occur) in experimental or *in vivo* settings. In some situations, the thrombus grew to occlude the vessel, bringing the fluid motion to a stop (Fogelson & Guy, 2004). In other situations, when the injury occurred in a region of high shear stresses, portions of the thrombus embolized (broke away) from the main thrombus in response to fluid stresses they were unable to support (Fogelson & Guy 2008).

Despite these successes, the single phase model has serious limitations which are consequences of the assumption that all species move in the same velocity field. One limitation is that without relative flow between the thrombus and the fluid bringing in additional platelets, the density of platelets in the thrombus can only slightly exceed the low density of platelets in the bulk fluid. This is unrealistic; platelets in thrombi reach densities as much as 100-fold greater than that in the bulk plasma. Another serious limitation is that the single phase model requires platelet activation and bond formation to occur unrealistically fast in order for a thrombus to form and remain attached to the injured plaque. For the thrombus to remain in place over the injured plaque in the single phase model, the fluid motion there has to be quickly brought to a halt; otherwise, the platelets in the thrombus are carried away by the moving fluid. Thus the model precludes studying thrombus formation at physiologically meaningful rates. In addition, the single phase model does not permit study of flow through a growing thrombus and its cessation as the density of platelets in the thrombus grows. Recent studies (Leiderman & Fogelson 2011, 2013; Stalker *et al.* 2013; Tomaiuolo *et al.* 2014; Welsh *et al.* 2014) have indicated that intraclot flow likely plays an important part in thrombus growth dynamics.

In an attempt to remove these limitations, we developed the two-phase model that we present in this article. In this model, we introduce a third population of platelets, those that are bound to other platelets. The individual unactivated and activated platelets move at the same velocity as the blood plasma. The bound platelets move at a different velocity. Both fluid and bound platelets may be present at each spatial

location and the model involves the volume fractions of the fluid phase and the bound platelet phase at each point. The bound platelet volume fraction can vary from zero to close to one.

Two sets of momentum equations govern the two velocity fields; each involves the stresses appropriate for the respective material. The fluid momentum equation takes account of viscous, pressure and drag forces due to relative motion between the fluid and bound platelets. The bound platelet momentum equation takes account of viscous, pressure, drag forces and the forces produced by interplatelet bonds. The last are determined by solving evolution equations for the platelet bond stress tensor $\underline{\underline{\sigma}}^{\mathrm{p}}$ and platelet bond concentration z_{b}. The multiphase platelet thrombosis model's equations are adapted from the generic multiphase equations we discussed in Wright *et al.* (2011) and the computational methods we use to solve these equations are extensions of those we developed for the more generic equations (Wright *et al.* 2008, 2011; Du *et al.* 2013). These methods can handle the challenges posed by substantial variations in volume fraction, including the degeneracy that occurs if one of the materials is absent in a region of space. They can handle the generalized Phan-Thien-Tanner-type (Tanner 2000) stress evolution equation needed to describe the stresses produced by evolving distributions of interplatelet bonds. The model and numerical methods can also handle a novel feature of the new model which is that individual platelet-platelet bonds must have nonzero rest length.

In the next section, we describe the two-phase platelet aggregation model in detail. Following that, we briefly describe our computational approach to solving the model's equations. Then we present the results of a range of computational simulations demonstrating the model's capabilities and behaviours and illustrating the strong differences in behaviour between the single phase model and the new multiphase one. An appendix provides more details on the derivation of the models equations.

2. Two-phase model for platelet aggregation

The model we propose involves three populations of platelets, an activating chemical which can cause a platelet to transition between populations, a bulk fluid, elastic bonds or links between the bound platelets and stresses produced by those links. In the next sections, we present the interactions and transitions in which platelets are involved; the equations which determine the velocity fields of the bulk fluid and of the bound platelets; the nature and evolution of the stresses produced by the elastic bonds, and the dynamics of elastic bond formation and breakage. The model is a 'macroscale' model in which quantities vary with the spatial variable $\mathbf{x}$ on a scale the size of the blood vessel diameter. This model may be derived from a model with two spatial scales in which a scaled microscopic spatial variable $\mathbf{y}$ is used for quantities which vary on the scale of a platelet diameter. The 'bond length' or the distance between the centres of two platelets bound to one another is one such quantity. The Appendix gives a sketch of the derivations of the macroscale model from the two-scale one.

2.1 *Platelet and chemical equations*

The model involves three populations of platelets: unactivated, activated (but unbound) and bound (and activated) with number densities ϕ_{u}, ϕ_{a} and ϕ_{b}, respectively. It also involves an activating chemical, with concentration c, which can cause unactivated platelets to become activated. In turn, this chemical is released by platelets into the bulk fluid as they become activated. Unactivated and activated (but unbound) platelets are individual tiny particles whose combined volume fraction is small. We assume that they have a negligible effect on the motion of the bulk fluid, that they advect at the velocity $\mathbf{u}_{\mathrm{f}}$ of the bulk fluid, and that their volume is part of that of the fluid. In contrast, bound platelets can form aggregates of considerable volume fraction and the bonds between them produce forces on the bound platelets when

those bonds' lengths differ from their equilibrium length. We introduce a second velocity field, $\mathbf{u}_\mathrm{b}$, at which the bound platelets move. Platelets transition between the unactivated and activated state at rate f_ua. Once activated, platelets do not again become unactivated. Activated platelets become bound at rate f_ab and bound platelets separate from other bound platelets to become individual activated platelets at rate f_ba. The platelet number densities, the activating chemical concentration and the two velocity fields are assumed to be functions of the spatial variable $\mathbf{x}$ and time t.

The equations governing the platelet number densities and the activating chemical concentration are

$$(\phi_\mathrm{u})_t + \nabla\cdot(\mathbf{u}_\mathrm{f}\phi_\mathrm{u}) = \nabla\cdot(D_\mathrm{u}\nabla\phi_\mathrm{u}) \; - f_\mathrm{ua} \tag{2.1}$$

$$(\phi_\mathrm{a})_t + \nabla\cdot(\mathbf{u}_\mathrm{f}\phi_\mathrm{a}) = \nabla\cdot(D_\mathrm{u}\nabla\phi_\mathrm{a}) \; + f_\mathrm{ua} + f_\mathrm{ba} - f_\mathrm{ab} \tag{2.2}$$

$$(\phi_\mathrm{b})_t + \nabla\cdot(\mathbf{u}_\mathrm{b}\phi_\mathrm{b}) = \qquad\qquad f_\mathrm{ab} - f_\mathrm{ba} \tag{2.3}$$

$$(c)_t + \nabla\cdot(\mathbf{u}_\mathrm{f}c) = \nabla\cdot(D_\mathrm{c}\nabla c) + Af_\mathrm{ua} - kc. \tag{2.4}$$

Here, D_u and D_c are the diffusion coefficients of the individual unbound platelets and the activating chemical, respectively, A is the amount of activating chemical released by each platelet that becomes activated, and kc is the rate of degradation of the activating chemical.

We assume that the activating chemical can only activate platelets when its concentration comes close to a prescribed threshold concentration c_T, and we set the activating rate function to

$$f_\mathrm{ua} = R(c)\phi_\mathrm{u} = R_0H(c - c_T)\phi_\mathrm{u}, \tag{2.5}$$

where R_0 is a constant, and $H(\cdot)$ is a smoothed version of the Heaviside step function. To describe the other platelet state transition functions requires the introduction of several additional quantities and is deferred until section 2.4.

2.2 *Momentum equations*

The two velocity fields $\mathbf{u}_\mathrm{f}$ and $\mathbf{u}_\mathrm{b}$ are governed by coupled momentum equations. In describing them, it is helpful to use the volume fraction of bound platelets θ_b and the volume fraction of fluid (including the individual unactivated and activated platelets) θ_f. Towards that end, we denote the volume of each platelet by v_p. Then the bound platelet volume fraction is related to the bound platelet number density according to

$$\theta_b = v_p\,\phi_\mathrm{b} \tag{2.6}$$

and the fluid volume fraction is defined by

$$\theta_f = 1 - \theta_b. \tag{2.7}$$

Letting $\tilde{\theta}_f$ denote the volume fraction of actual bulk fluid (not including unactivated and activated platelets), it then follows that $\tilde{\theta}_f$ satisfies the equation

$$(\tilde{\theta}_f)_t + \nabla\cdot(\mathbf{u}_\mathrm{f}\tilde{\theta}_f) = -\nabla\cdot(D_\mathrm{u}\nabla\phi_\mathrm{u}) - \nabla\cdot(D_\mathrm{u}\nabla\phi_\mathrm{a}). \tag{2.8}$$

where the terms on the right-hand side reflect the displacement of actual fluid by diffusing single platelets. Multiplying each of Equations 2.1–2.3 by v_p and combining the resulting equations with Equation 2.8, we find that

$$\nabla\cdot(\theta_f \mathbf{u}_\mathrm{f} + \theta_b \mathbf{u}_\mathrm{b}) = 0. \tag{2.9}$$

We refer to this equation as the co-incompressibility equation. It is a constraint on the volume-fraction averaged velocity. Anywhere that θ_f and θ_b are both nonzero, neither individual velocity field $\mathbf{u}_\mathrm{f}$ and $\mathbf{u}_\mathrm{b}$ need be incompressible, but this average velocity field must be.

We assume that the bulk fluid behaves as a Newtonian fluid that is subject to drag due to relative motion between it and the bound platelets. The relevant momentum equation is then

$$(\theta_\mathrm{f}\mathbf{u}_\mathrm{f})_t + \nabla\cdot(\theta_\mathrm{f}\mathbf{u}_\mathrm{f}\mathbf{u}_\mathrm{f}) = -\theta_\mathrm{f}\nabla p + \nabla\cdot(\theta_\mathrm{f}\underline{\underline{\sigma}}^{\mathrm{fv}}) + \xi\theta_\mathrm{f}\theta_\mathrm{b}(\mathbf{u}_\mathrm{b} - \mathbf{u}_\mathrm{f}). \tag{2.10}$$

The bound platelet material is also assumed to behave as a Newtonian fluid with drag due to relative motion between the bound platelets and the bulk fluid, and we assume it is also affected by stresses coming from the elastic bonds between bound platelets. Its momentum equation is

$$(\theta_\mathrm{b}\mathbf{u}_\mathrm{b})_t + \nabla\cdot(\theta_\mathrm{b}\mathbf{u}_\mathrm{b}\mathbf{u}_\mathrm{b}) = -\theta_\mathrm{b}\nabla p + \nabla\cdot(\theta_\mathrm{b}\underline{\underline{\sigma}}^{\mathrm{bv}}) + \nabla\cdot(\theta_\mathrm{b}\underline{\underline{\sigma}}^{\mathrm{b}}) + \xi\theta_\mathrm{f}\theta_\mathrm{b}(\mathbf{u}_\mathrm{f} - \mathbf{u}_\mathrm{b}). \tag{2.11}$$

In Equations 2.10 and 2.11, $\underline{\underline{\sigma}}^{\mathrm{fv}}$ and $\underline{\underline{\sigma}}^{\mathrm{bv}}$ are the viscous stress tensors for the bulk fluid and bound platelet material, respectively. The quantity p is a Lagrange multiplier which we refer to as pressure whose role is to enforce the co-incompressibility condition Equation 2.9. The term $\xi\theta_\mathrm{f}\theta_\mathrm{b}(\mathbf{u}_\mathrm{f} - \mathbf{u}_\mathrm{b})$ is the force exerted on the bound platelets due to drag between them and the bulk fluid (the drag coefficient ξ will be specified below). The quantity $\underline{\underline{\sigma}}^{\mathrm{b}}$ is the stress tensor due to bonds between bound platelets; its evolution is discussed in the next section.

The Newtonian viscous stress tensors are defined by the equations

$$\underline{\underline{\sigma}}^{\mathrm{fv}} = \mu_\mathrm{f}\left(\nabla\mathbf{u}_\mathrm{f} + \nabla\mathbf{u}_\mathrm{f}{}^T\right) + (\lambda_\mathrm{f}\nabla\cdot\mathbf{u}_\mathrm{f})\underline{\underline{I}} \tag{2.12}$$

$$\underline{\underline{\sigma}}^{\mathrm{bv}} = \mu_\mathrm{b}\left(\nabla\mathbf{u}_\mathrm{b} + \nabla\mathbf{u}_\mathrm{b}{}^T\right) + (\lambda_\mathrm{b}\nabla\cdot\mathbf{u}_\mathrm{b})\underline{\underline{I}}, \tag{2.13}$$

where $\underline{\underline{I}}$ is the identity tensor, $\mu_{\mathrm{b,f}}$ are the shear viscosities and $\lambda_{\mathrm{b,f}} + 2\mu_{\mathrm{b,f}}/d$ are the bulk viscosities of the bound platelets and bulk fluid (d is the spatial dimension), respectively. We choose $\lambda_{\mathrm{b,f}} = -\mu_{\mathrm{b,f}}$ so that the bulk viscosities in both phases are zero.

2.3 *Stress due to platelet–platelet bonds*

To describe the stresses due to molecular bonds between bound platelets, we begin by introducing the quantity $z_\mathrm{b}(\mathbf{x}, t)$ defined as the number density of platelet-platelet bonds at time t connecting bound platelets at location $\mathbf{x}$ to bound platelets anywhere. As derived in the Appendix, this quantity evolves according to the equation

$$(z_\mathrm{b})_t + \nabla\cdot(\mathbf{u}_\mathrm{b} z_\mathrm{b}) = \alpha(\phi_\mathrm{a}, \phi_\mathrm{b}) - \beta z_\mathrm{b}, \tag{2.14}$$

where $\alpha(\phi_\mathrm{a}, \phi_\mathrm{b})$ is the rate of bond formation and β is the bond breaking rate function. These functions are described in detail in section 2.4.

In Fogelson (1992) and Fogelson & Guy (2004), we derived the following evolution equation for $\underline{\underline{\sigma}}^{\mathrm{b}} = \underline{\underline{\sigma}}_0^{\mathrm{b}}$ from a more fundamental two-scale model in which each bond between platelets acted as a linear spring with rest-length zero (the subscript 0 indicates the rest length):

$$(\underline{\underline{\sigma}}_0^{\mathrm{b}})_t + \nabla\cdot(\mathbf{u}_{\mathrm{b}}\underline{\underline{\sigma}}_0^{\mathrm{b}}) = \underline{\underline{\sigma}}_0^{\mathrm{b}}\underline{\underline{\nabla\mathbf{u}_{\mathrm{b}}}} + (\underline{\underline{\sigma}}_0^{\mathrm{b}}\underline{\underline{\nabla\mathbf{u}_{\mathrm{b}}}})^T + C_1\alpha(\phi_{\mathrm{a}},\phi_{\mathrm{b}})\underline{\underline{I}} - \beta\underline{\underline{\sigma}}_0^{\mathrm{b}}. \tag{2.15}$$

where C_1 is a constant as defined in Equation A.22 in the Appendix. In Fogelson (1992), we showed that Equations 2.14 and 2.15 are *exact* consequences of the two-scale model's equations if the breaking rate for bonds, β, constant. In Fogelson & Guy (2004), we showed that these equations hold approximately, under an appropriate closure approximation, even if the breaking rate β depends on the bond length. In the two-scale model, the bond length is represented by the magnitude of the microscale spatial variable $\mathbf{y}$. To form the closure, we needed a macroscale surrogate for the bond length, and we showed that

$$< |\mathbf{y}|^2 > (\mathbf{x},t) = \frac{2}{S_0}\frac{\mathrm{Tr}(\underline{\underline{\sigma}}_0^{\mathrm{b}}(\mathbf{x},\mathrm{t}))}{z_{\mathrm{b}}(\mathbf{x},t)}, \tag{2.16}$$

where the average is over the current distribution of bonds between bound platelets at $\mathbf{x}$ and other bound platelets, S_0 is the stiffness constant for a single bond, and Tr denotes the trace operator. We obtained the approximate closure by making β a suitable function of $\sqrt{< |\mathbf{y}|^2 >}$, calculated using Equation 2.16, rather than one of $|\mathbf{y}|$. (See Guy 2004a,b, for analysis and comparison of the behaviour of the closure model with that of the two-scale model)

Equation. 2.15 predicts that in steady-state and without fluid motion, $\underline{\underline{\sigma}}_0^{\mathrm{b}} = \frac{C_1\alpha}{\beta}\underline{\underline{I}}$ is a suction pressure. In our previous single-phase platelet model (Fogelson 1992; Fogelson & Guy, 2004), this 'platelet pressure' was balanced by a fluid pressure that preserved the incompressibility of the single velocity field in that model. In the context of our current two-phase model where the bound platelet velocity $\mathbf{u}_{\mathrm{b}}$ is, in general, not incompressible, this pressure would drive a bound-platelet motion that would collapse an aggregate to a point. To avoid this highly undesirable behaviour, we consider bonds which are linear springs with *nonzero* rest-length R. We show in the Appendix that the following expression gives an approximation to the stresses produced by such bonds. It is this approximation that we take as the definition of the bond stresses $\underline{\underline{\sigma}}^{\mathrm{b}}$ in this article.

$$\underline{\underline{\sigma}}^{\mathrm{b}} = \left(1 - R\sqrt{\frac{S_0 z_{\mathrm{b}}}{2\mathrm{Tr}(\underline{\underline{\sigma}}_0^{\mathrm{b}})}}\right)\underline{\underline{\sigma}}_0^{\mathrm{b}}. \tag{2.17}$$

Note that to calculate $\underline{\underline{\sigma}}^{\mathrm{b}}(\mathbf{x},t)$, it suffices to be able to calculate $\underline{\underline{\sigma}}_0^{\mathrm{b}}(\mathbf{x},t)$ and $z_{\mathrm{b}}(\mathbf{x},t)$ which we do using Equations 2.14 and 2.15. We elaborate on the bond formation function $\alpha(\phi_{\mathrm{a}},\phi_{\mathrm{b}})$ below. Further discussion of the platelet bond stresses can be found in the Appendix.

2.4 *Bond formation and breaking and platelet transitions*

Bonds can form between a pair of activated platelets, between an activated platelet and a bound platelet, and between a pair of bound platelets. For the first two of these, two and one platelets, respectively, transition between the activated and bound platelet populations. For the clot to be able to grow in size, an activated platelet must be able to bind to it at some small distance. As described in this section, we adapt a mechanism introduced in Leiderman & Fogelson (2011) to accomplish this. Bonds between a pair of

bound platelets can break. If a bond that breaks is the last one connecting one of the platelets to other bound platelets, then the platelet transitions from the bound to the activated platelet population. In our continuum model, we do not track discrete bonds between pairs of platelets, so we derive a procedure for assessing the probability that a bond that breaks is the last bond holding a platelet to other bound platelets. This is described at the end of this section.

We assume that each activated platelet has sites to form up to $n_{\mathrm{b}}^{\max}$ bonds with other platelets. Since each bond occupies two of these binding sites (one on each of the platelets it connects), the number density of unoccupied binding sites on already bound platelets is $A_{bs} = n_{\mathrm{b}}^{\max}\phi_{\mathrm{b}} - 2z_{\mathrm{b}}$. The density of unoccupied sites on activated but not yet bound platelets is $n_{\mathrm{b}}^{\max}\phi_{\mathrm{a}}$. We define the bond formation function α in Equations (2.14) and (2.15) as:

$$\alpha(\phi_{\mathrm{a}}, \phi_{\mathrm{b}}) = K_{aa}^{coh}(n_{\mathrm{b}}^{\max}\phi_{\mathrm{a}})^2 + K_{ab}^{coh}(n_{\mathrm{b}}^{\max}\phi_{\mathrm{a}})\eta + K_{bb}^{coh}\eta^2, \tag{2.18}$$

where K_{aa}^{coh}, K_{ab}^{coh} and K_{bb}^{coh} are second-order bond formation rate constants. In Equation (2.18), we have introduced the binding affinity function η which we assume satisfies the diffusion reaction equation:

$$\eta_t = D_{\mathrm{a}}\Delta\eta - k_{bs}\eta + k_{bs}A_{bs}\ . \tag{2.19}$$

This equation incorporates our assumption that the binding affinity at $\mathbf{x}$ is produced with a rate k_{bs} by each unoccupied binding site, decays with the same rate and diffuses with coefficient D_{a}. By choosing D_{a} and k_{bs} appropriately, η will be approximately zero except within a distance $d_b = O(\sqrt{D_{\mathrm{a}}/k_{bs}})$ of already bound platelets. The variable η gives a measure of the average number density of unoccupied binding sites on bound platelets within distance d_b of location $\mathbf{x}$. Use of η in Eq. (2.18) allows bonds to form between activated or bound platelets at $\mathbf{x}$ and bound platelets within distance d_b of $\mathbf{x}$ (Leiderman & Fogelson 2011).

Those new bonds involving activated platelets are accompanied by a transfer of activated platelets to the bound platelet population. Hence, the function f_{ab} in Eqations (2.2) and (2.3) is given by

$$f_{\mathrm{ab}} = 2C_3K_{aa}^{coh}(n_{\mathrm{b}}^{\max}\phi_{\mathrm{a}})^2 + C_3K_{ab}^{coh}(n_{\mathrm{b}}^{\max}\phi_{\mathrm{a}})\eta. \tag{2.20}$$

Setting $C_3 = 1$ is equivalent to assuming one bond is sufficient to bind an activated platelet to another platelet. If we set $C_3 < 1$, we are assuming that it takes $\frac{1}{C_3}$ bonds to initially bind the platelets together.

According to Equation (2.14), bonds break at rate βz_{b}. The rate at which bound platelets become (unbound) activated platelets is then $\beta z_{\mathrm{b}}P_1$ where P_1 is the probability that a bond that breaks is the last one for a platelet. To determine P_1 we proceed as follows. First note that $n_{\mathrm{b}}(\mathbf{x}, t) = \frac{z_{\mathrm{b}}}{\phi_{\mathrm{b}}}$ is the average number of bonds per bound platelet at $\mathbf{x}$. Let $P(n;\lambda)$ denote the Poisson distribution with mean λ. Suppose that the number of bonds for a bound platelet is distributed over $n = 1, 2, 3...$ (n cannot be 0 for a bound platelet) according to a modified Poisson distribution

$$\tilde{P}(n;\lambda) = \frac{P(n;\lambda)}{(1 - e^{-\lambda})}.$$

Then the probability that $n = 1$ is

$$\tilde{P}(1;\lambda) = \frac{P(1;\lambda)}{1 - e^{-\lambda}} = \frac{\lambda}{e^{\lambda} - 1}. \tag{2.21}$$

To determine λ, we require that the expected value of n under the distribution $\tilde{P}$ is n_b, i.e.

$$n_\mathrm{b} = \frac{\lambda}{1 - e^{-\lambda}}. \tag{2.22}$$

To summarize, for each $\mathbf{x}$ and t, we determine λ by solving Equation (2.22) with $n_\mathrm{b}(\mathbf{x}, t) = z_\mathrm{b}(\mathbf{x}, t)/\phi_\mathrm{b}(\mathbf{x}, t)$, and then we set

$$f_\mathrm{ba} = \beta z_\mathrm{b} P_1(n_\mathrm{b}), \tag{2.23}$$

where $P_1(n_\mathrm{b}) \equiv \tilde{P}(1; \lambda)$.

In defining the breaking rate function β, we follow Fogelson & Guy (2004) and make it a function of $w \equiv \frac{\mathrm{Tr}(\boldsymbol{\sigma}^\mathrm{b}_{=0})}{z_\mathrm{b}}$, because this quantity is related to the local average bond length as discussed above (see Equation (2.16)). The specific function we use is

$$\beta = \begin{cases} \beta_0 & \text{if } w \le w^* \\ \beta_0(1 + \frac{\gamma}{R}(w - w^*)) & \text{if } w > w^*, \end{cases} \tag{2.24}$$

where $w^* = \frac{S_0}{2}R^2$ and β_0 and γ are specified constants. That is, we assume that for bonds with length larger than the bond rest length R, the breaking rate increases linearly with the mean-squared bond length.

2.5 *Drag coefficient*

It remains to define the coefficient ξ in the expression $\xi\theta_\mathrm{f}\theta_\mathrm{b}(\mathbf{u}_\mathrm{f} - \mathbf{u}_\mathrm{b})$ for the drag between the bulk fluid and the bound platelets. If ξ were constant, the drag at a location would be zero if either of these materials were not present there, but the dependence on θ_b for intermediate values of θ_b would be fairly weak. There is good evidence that the permeability of platelet aggregates decreases dramatically as the platelet volume fraction grows toward ≈ 0.6 (Wufsus *et al.* 2013). To account for this observation, we make ξ a function of the bound platelet volume fraction θ_b. For low values of θ_b, the aggregate forms a loose porous structure that only weakly impedes motion of fluid through it. For such situations we want ξ to be small. As the density of platelets within an aggregate grows, its porosity decreases and it offers more resistance to fluid permeation. As θ_b gets close to a maximal packing density, ξ should become very large. The specific function we use for the simulations in this article is

$$\xi(\theta_\mathrm{b}) = \xi_0 + \frac{10^7}{1 + e^{-60(\theta_\mathrm{b} - \theta_\mathrm{b}^{\max})}}, \tag{2.25}$$

where $\theta_\mathrm{b}^{\max}$ is the prescribed maximum volume fraction of bound platelets ($\theta_\mathrm{b}^{\max} = 0.6$ is used for all results in the article). Figure 1 shows a plot of this function plot of ξ as a function of the bound platelet volume fraction θ_b for $\theta_\mathrm{b}^{\max} = 0.6$ and $\xi_0 = 0$.

3. Computational methods

A staggered Marker-and-Cell (MAC) grid is used to represent discrete values of the variables. The components of the velocity vectors are located at the centres of cell edges and all other variables are located at cell centres.

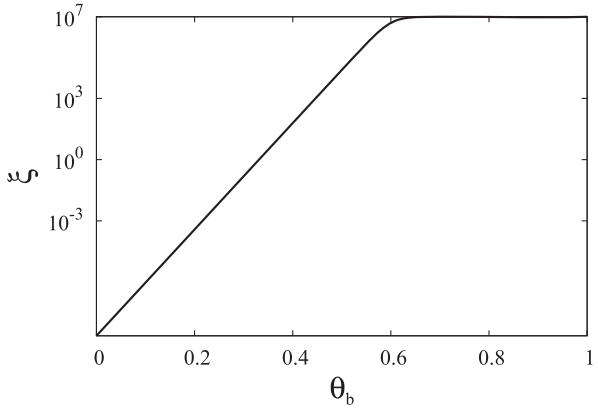

FIG. 1. Drag coefficient ξ *vs* bound platelet volume fraction θ_b.

1. With the given values for ϕ_a, ϕ_b, $\underline{\underline{\sigma}}^b$ and z_b, solve a discrete version of Equations (2.9)–(2.11) to get $\mathbf{u}_f$ and $\mathbf{u}_b$.
2. Ignoring the reaction terms, solve discrete versions of the advection-diffusion parts of Equations (2.1)–(2.4) to update ϕ_u, ϕ_a, ϕ_b and c.
3. Update ϕ_u, ϕ_a, ϕ_b and c to account for the reaction terms in Equations (2.1)–(2.4).
4. Solve a discrete analogue of Equations (2.14) and (2.15) with the velocity field $\mathbf{u}_b$, ϕ_a and ϕ_b computed from the two previous steps.
5. Repeat until final time is reached.

In step 1, a multigrid preconditioned GMRES solver is used to solve the system of equations (Wright *et al.* (2011)). Note that since ϕ_b is nonzero only in part of the domain, $\theta_b = 0$ in the complementary domain and the network momentum equation (2.11) becomes degenerate there. To avoid this difficulty, we regularize the discrete equations by temporarily increasing θ_b by a small positive constant when setting up the discrete linear equations, and then we solve the same set of equations everywhere throughout the entire domain (Du *et al.* (2013)). For the remaining equations, all of the advection terms are discretized explicitly in time by the second-order corner transport upwind scheme as described in Colella (1990) and a Crank–Nicolson approximation is used for the diffusion terms. A second order Runge–Kutta solver is used to solve the ordinary differential equations that account for the reaction terms.

4. Results

4.1 *Test of the two-phase algorithm: grab and pull experiment*

The 'grab and pull' experiment was used in Wang & Fogelson (1999) and Guy (2004a) for the single phase model of platelet aggregation which does not allow relative motion of the platelets and fluid. The computational domain is a periodic unit square $[-0.5, 0.5] \times [-0.5, 0.5]$ with a single phase viscous fluid inside. A background force is applied to drive a four-mill-type stagnation-point flow. Initially the number density of unactivated platelets is $\phi_u = 1$ everywhere. Activation chemical is added within a circle of radius $r = 0.125$ centred at the stagnation point to activate ϕ_u and bonds start to form. At time $t = 0.1$, further activation is shut off and extra forces are applied in the x-direction in an attempt to break the platelet aggregate. See Guy (2004a) for more details about the test.

Here we carry out the grab and pull test with the two-phase model to illustrate the important effects of relative motion in the problem. The values of viscosity for bound platelets and fluid are $\mu_b = \mu_f = 0.04$. We set the volume of a single platelet to be $v_p = 0.1$. Both the background force and the extra pulling force are distributed to bound platelets and fluid in proportion to their volume fractions. In the first test, we use a large baseline drag coefficient $\xi_0 = 10^8$ so that bound platelet and fluid move together. In the second test, we choose $\xi_0 = 0.01$ so there can be significant relative motions between the platelet aggregate and the surrounding fluid when the volume fraction of bound platelet is relatively low. The results are plotted in Fig. 2. Here the colour plot is the distribution of the bond density z_b and the vector field is the velocity $\mathbf{u}_b$ of bound platelets. For the case with large drag (left column of the figure), the largest value of the bound platelet number density is about 0.92, which is less than the initial concentration of unactivated platelet. Since everything moves at about the same velocity which is divergence free, there can be no local accumulation of platelet through advection. During the whole process, the viscoelastic force generated by the platelet bonds is always less than the pulling force, hence the bound platelets are pulled apart in an accelerating manner (i.e. $\mathbf{u}_b$ increases in t). The platelet aggregate is completely broken into two pieces at time $t = 0.35$, and the pieces are significantly deformed by the background force ($t = 0.475$).

The situation is very different for the test when the baseline drag coefficient is low. As seen in Fig. 2(b), at the early stage $t = 0.175$, the aggregate is compressed vertically and stretched horizontally, as in the case with large drag. Since the bound platelet aggregate is still quite porous (maximum bound platelet volume fraction $\theta_b = 0.1$) at this stage, the frictional drag force is small and fluid can easily pass through the aggregate without much interference. Due to the weak interactions with the fluid, the bound platelets move much more slowly than do those under large drag (Fig. 2(a)). As the fluid motion brings additional unactivated platelets (ϕ_u) into the bound platelet aggregate and they are activated and bind, the aggregate becomes much denser, with largest values of ϕ_b reaching 4.5 and 5.8 in Fig. 2(d) and (f), respectively. For $v_p = 0.1$, these values correspond to bound platelet volume fraction θ_b values of 0.45 and 0.58. Because the drag coefficient is a sharply increasing function of θ_b, the drag force increases dramatically and the flow of fluid through the aggregate decreases greatly. With the increase of the number density of bound platelets, more bonds are formed to resist the stretching. At time $t = 0.35$, values of both z_b and ϕ_b are much higher than in the large drag test and the aggregate produces stresses sufficiently large to keep it in one piece. As the bonds continue to break, it takes a much longer time to pull the aggregate apart completely ($t = 0.475$). Compared with the test with large drag, the overall deformation of the aggregate is much less.

4.2 *Simulation of platelet aggregation with two-phase model*

In this section, we present computational results for platelet aggregation within a two-dimensional flow channel. The channel has height of 0.5 cm and length of 3.5 cm. A 32×224 uniform rectangular computational grid is used for all simulations. With a grid of this size, a typical simulation takes around 24 hours on a computer with Dual-Core AMD Processors (1.0 GHz). Simulations on finer grids give very similar results. For all the simulations, both velocities $\mathbf{u}_f$ and $\mathbf{u}_b$ satisfy no-slip conditions at the top and bottom vessel walls. Homogeneous Neumann conditions are applied to them at the inlet and outlet. A constant background force is applied in the positive x-direction so that a parabolic flow with largest velocity of 5.0 cm/s would be generated in the absence of bound platelets. This corresponds to a wall shear rate of 40s^{-1}. All the results in section 4.2.1–4.2.3 are based on this wall shear rate. In section 4.2.4, we investigate the effects of shear rate on thrombus growth. Initially, $\phi_u = 1$ throughout the domain and ϕ_a, ϕ_b, c, $\underline{\underline{\sigma}}^b$ and z_b are set to zero. Dirichlet boundary conditions $\phi_u = 1$, $\phi_a = \phi_b = c = z_b = 0$ and $\underline{\underline{\sigma}}^b = 0$ are imposed at the inlet and homogeneous Neumann conditions are imposed for these quantities

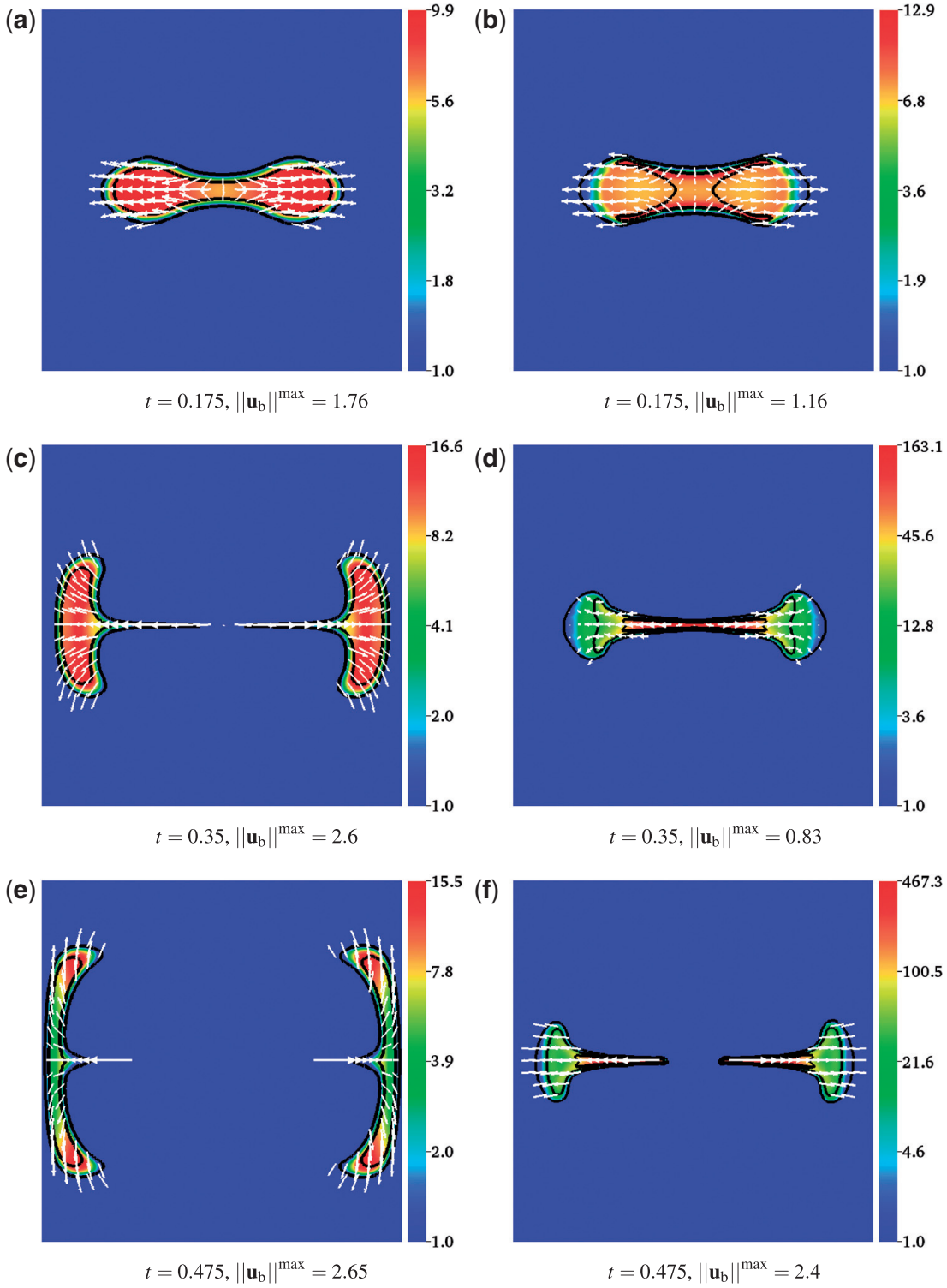

FIG. 2. Bond density z_b and bound platelet velocity $\mathbf{u}_b$. Left: $\xi_0 = 10^8$ and black contour lines are for $\phi_b = 0.1$ (outer one) and 0.9 (inner one). Right: $\xi_0 = 0.01$ and black contour lines are $\phi_b = 0.1$, 0.9 and 2 (from outside to inside, contour lines for $\phi_b = 2$ are for (d) and (f) only). All velocity vectors have the same scale.

TABLE 1 *Summary model parameters*

Parameter	Value	Parameter	Value
μ_{f}	0.04 g cm^{-1}s^{-1}	R_0	2.0 s^{-1}
μ_{b}	4.0 g cm^{-1}s^{-1}	K_{aa}^{coh}, K_{ab}^{coh}, K_{bb}^{coh}	0.6 cm^3 s^{-1}
D_u	10^{-7} cm^{2}s^{-1}	C_1	4.0 g cm^{2}s^{-2}
D_c	5.0×10^{-6} cm^{2}s^{-1}	C_3	$\frac{1}{12}$
D_a	10^{-4} cm^{2}s^{-1}	β_0	0.05 s^{-1}
k	0.05 s^{-1}	γ	2.0
k_{bs}	10.0 s^{-1}	v_p	0.1 cm^3
A	12.0	$n_{\mathrm{b}}^{\max}$	30.0

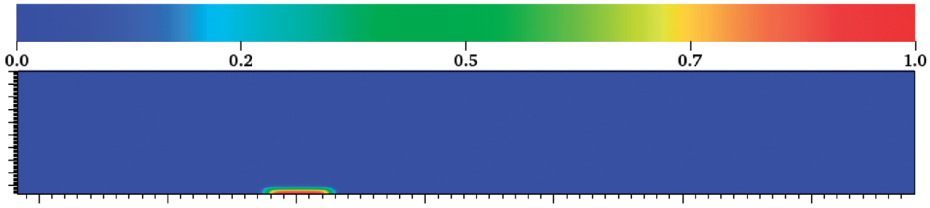

FIG. 3. The injury zone with the distribution of R_{iz}. Channel has height of 0.5 cm and length of 3.5 cm.

at the outlet. For the rest of the article, the parameter values listed in Table 1 are used unless otherwise indicated. In the table, some values such as μ_{f} and D_u are set according to experimental data. Others are chosen to explore the capabilities of the model.

In this work, we do not model the complicated biochemical and mechanical interactions between the platelets and the vessel walls. Instead, to start the aggregation process, we introduce an 'injury zone' near the vessel wall in which unactivated platelets are activated at a specified rate (Guy, 2004a). The platelet activation function f_{ua} is modified to include activation in the injury zone: $f_{\mathrm{ua}} = (R(c) + R_{iz}(\mathbf{x}))\phi_{\mathrm{u}}$. Here, the function $R_{iz}(\mathbf{x})$ is chosen such that its value decays rapidly from the centre of its support located at $(0, 0)$. As plotted in Fig. 3, the support of the injury is approximately 0.3 long horizontally and 0.05 long vertically. The bond formation constant k_{aa}^{coh} is scaled by R_{iz} so that outside of the injury zone, binding between activated but unbound platelets (ϕ_{a}) is negligible.

4.2.1 *Thrombus growth with flow* First we choose a relatively small baseline drag coefficient $\xi_0 = 0.1$ in Equation (2.25) so that there can be significant relative motion between the fluid and the bound platelets. The bound platelet density function ϕ_{b} and the fluid velocity field $\mathbf{u}_{\mathrm{f}}$ at different stages of the simulation are shown in Fig. 4(a–d). At an early time $t = 16$ s, when θ_{b} is much less than $\theta_{\mathrm{b}}^{\max}$ in most of the thrombus, fluid can easily permeate the platelet aggregate and the overall flow field is perturbed only a little. As the background flow brings in more unactivated platelets which become activated and bind to the existing platelet aggregate, ϕ_{b} increases and the thrombus becomes denser, especially near its upstream edge (Fig. 4 (b) and (c)). The fluid velocity $\mathbf{u}_{\mathrm{f}}$ becomes much smaller within the region with densely packed platelets and the flow is diverted around the growing thrombus. By $t = 88$, the thrombus has grown significantly in both the vertical and the horizontal directions, and occludes more than 50% of the vessel lumen. The thrombus contains a flow-resistant dense core surrounded by a more porous outside

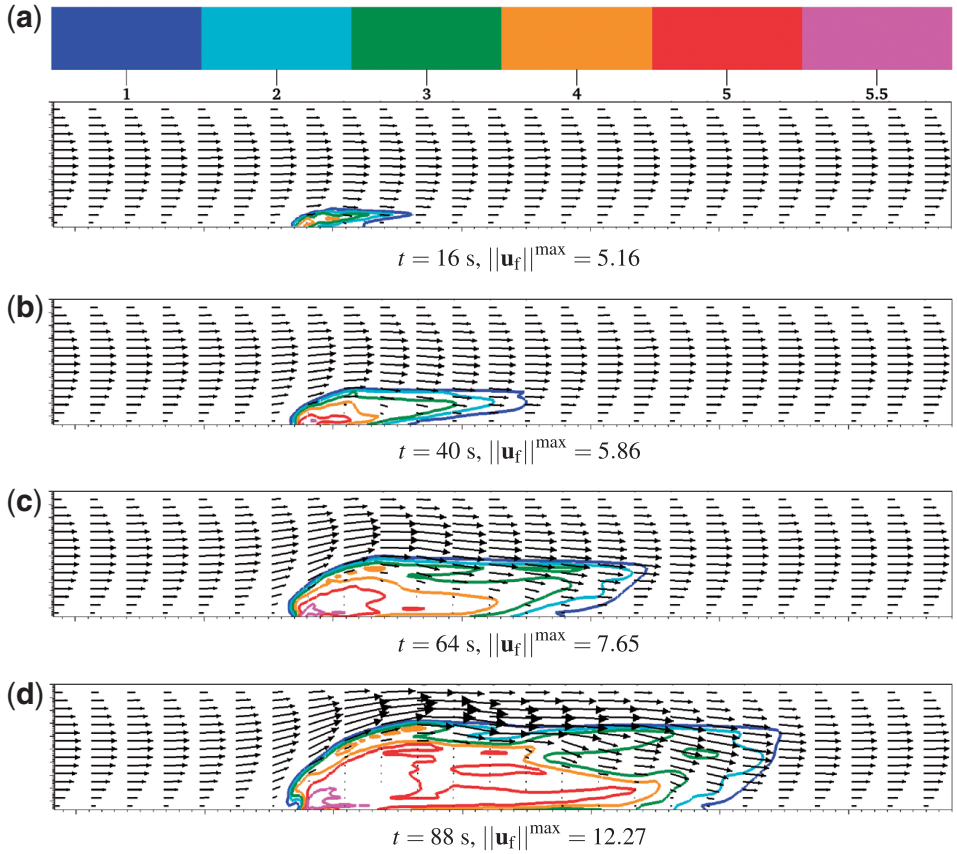

FIG. 4. Bound platelet density ϕ_b and fluid velocity $\mathbf{u}_f$ at different time for $\xi_0 = 0.1$. All vectors have the same scale. The volume fraction of bound platelet varies from 0 to 5.8.

layer through which fluid can move. A similar core-shell thrombus structure was observed in *in vivo* experiments (van Gestel *et al.* 2002; Stalker *et al.* 2013). Interestingly, the dense core encompasses the injury site and the growth of the thrombus is mainly in the downstream direction. The largest value of the bound platelet number density within the thrombus is about $\phi_b = 5.8$, a value which is significantly higher than the number density of unactivated platelets in the bulk flow $\phi_u = 1.0$.

The distributions of activator chemical c and the unactivated and activated platelet number densities, ϕ_u and ϕ_a, respectively at $t = 64$ s are plotted in Fig. 5(a–c). The black contour line shows $\phi_b = 1$ and the white dashed line in Fig. 5(a) is the threshold concentration of chemical above which platelets are activated. It can be seen from Fig. 5(b) that at spatial locations where the chemical concentration is above threshold, ϕ_u is low indicating that most of the unactivated platelets have become activated. As shown in Fig. 5(c), moving from the edge to the interior of the aggregate, the value of ϕ_a decreases significantly. Within the thrombus where $\mathbf{u}_f$ is relatively small, the majority of activated platelets become bound because of their long period of interaction with locally available binding sites and consequently ϕ_a is relatively low and ϕ_b is relatively high. In contrast, near the top edge of the aggregate where the fluid motion is much faster, activated platelets may be washed away before they become bound. The distributions of the bond density z_b and the bound platelet velocity $\mathbf{u}_b$ are shown in Fig. 6(a). We see that z_b exhibits a core-shell structure, similar to that for bound platelets, with high values of the bond density at locations where ϕ_b is large. The largest values of z_b are close to their quasi-steady state values $\frac{n_b^{max}\phi_b}{2}$.

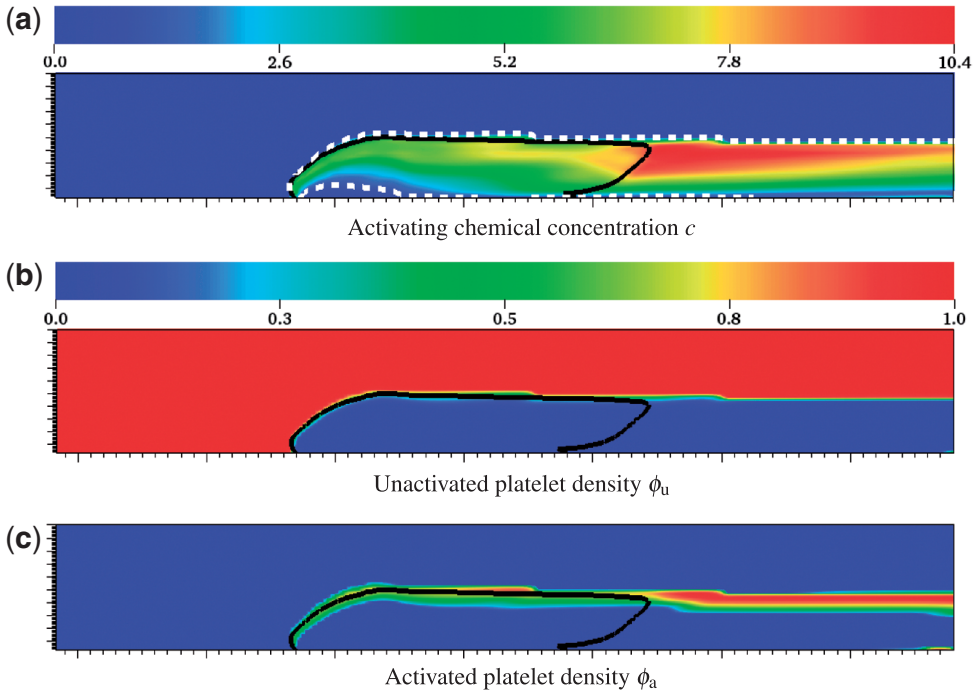

FIG. 5. Activating chemical concentration c and unactivated and activated platelet number densities, ϕ_u and ϕ_a, respectively, at $t = 64$ s. The black contour is for bound platelet density $\phi_b = 1$. The white dashed contour in (a) is for chemical concentration $c = 1$.

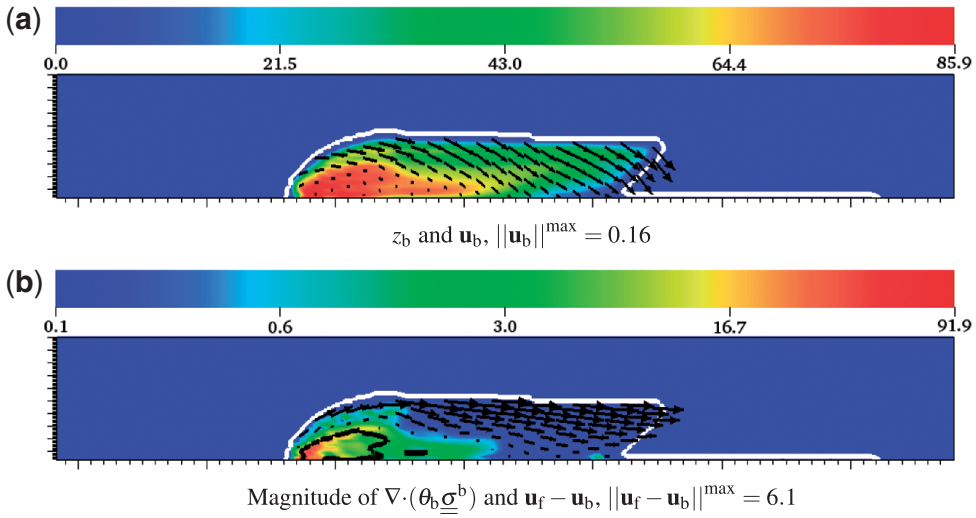

FIG. 6. At $t = 64$ s, (a) bond density z_b and bound platelet velocity $\mathbf{u}_b$, (b) magnitude of viscoelastic force $\nabla \cdot (\theta_b\underline{\underline{\sigma}}^b)$ and relative velocity $\mathbf{u}_f - \mathbf{u}_b$. The white contour is for $\phi_b = 0.001$

For bound platelets, the outside porous layer moves much more rapidly than the dense inner core. Notice that at the upstream edge of the aggregate, the motion of bound platelets is towards the dense core, thus contributing to enlarging the core region. In Fig. 6(b), the magnitude of the viscoelastic force $\nabla\cdot(\theta_b\underline{\underline{\sigma}}^b)$ produced by the platelet bonds is plotted together with the relative velocity $\mathbf{u}_f - \mathbf{u}_b$. The black contour line indicates where $\phi_b = 5$. The largest value of the viscoelastic force appears at the upstream end of the

thrombus and coincides approximately with the boundary of the dense core of bound platelets. Within the more porous region of the thrombus where the fluid drag is small, the bonds between platelets are less stretched and thus the viscoelastic force they produce is relatively small. It is exactly within this region that the fluid and bound platelets have the most significant relative motion. We note that, because of the regularization used for θ_b where it is very small (section 3), we plot vectors $\mathbf{u}_b$ and $\mathbf{u}_f - \mathbf{u}_b$ only for region in which $\phi_b \geq 0.001$. This applies to all results presented in this article.

4.2.2 *Effects of fluid drag on thrombus growth* In this section, we look at the effect of fluid drag on the growth of a thrombus. For these simulations, we increased the bound formation rates K_{aa}^{coh}, K_{ab}^{coh} and K_{bb}^{coh} from 0.6 to 0.7 while changing the value of C_3 from $\frac{1}{12}$ to $\frac{1}{14}$ to leave unchanged the products $C_3K_{aa}^{coh}$ and $C_3K_{ab}^{coh}$ in the bound platelet creation function f_{ab}. This is tantamount to assuming that more bonds are formed each time an activated platelet first becomes bound. Consequently, subsequent binding of activated platelets to the existing thrombus occurs more slowly because the density of available binding sites on bound platelets is smaller. We carried out simulations with three baseline drag coefficient values $\xi_0 = 10, 100$, and 10^6. As shown in Fig. 7(a–c), the change of ξ_0 has a dramatic impact on thrombus formation. For $\xi_0 = 10$, the result is similar to those presented in the previous section. The thrombus grows both vertically and horizontally with a clear core-shell structure. With an increase of ξ_0 to 100, the thrombus exhibited more growth in the downstream direction and less vertical growth. A small piece of the loose-shell outer portion of the thrombus was dislodged by fluid drag and washed downstream. Simulation results at later times (not shown) indicate that such embolization happens frequently, and this has the effect of greatly limiting the thrombus' growth. When ξ_0 is further increased to $\xi_0 = 10^6$, there is a significant increase in the thrombus growth rate, both in the vertical and horizontal directions. In this

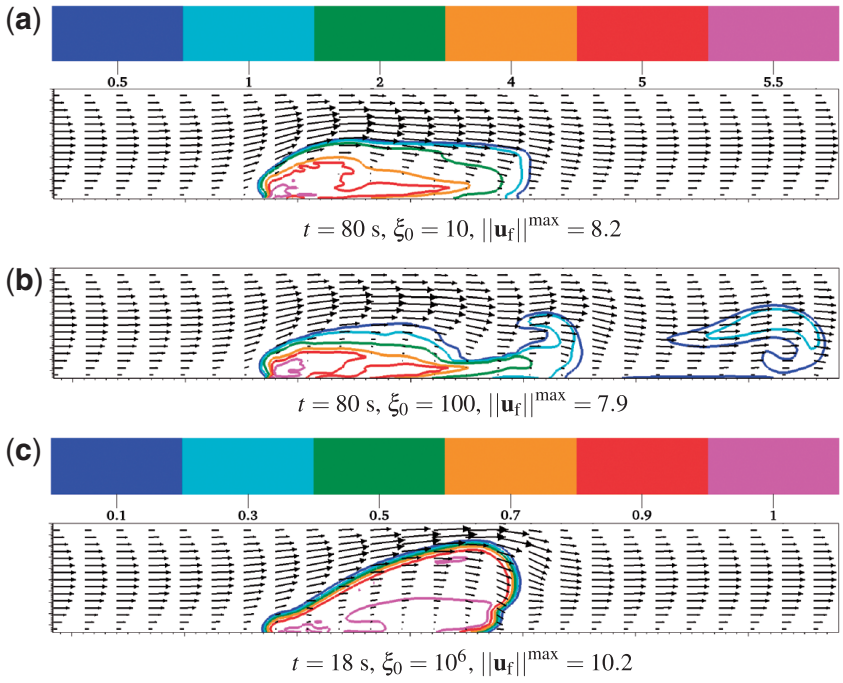

FIG. 7. Bound platelet density ϕ_b and fluid velocity $\mathbf{u}_f$ for different baseline drag ξ_0. Here (a) and (b) are at $t = 80$ s and (c) is at $t = 18$ s. All vectors have the same scale.

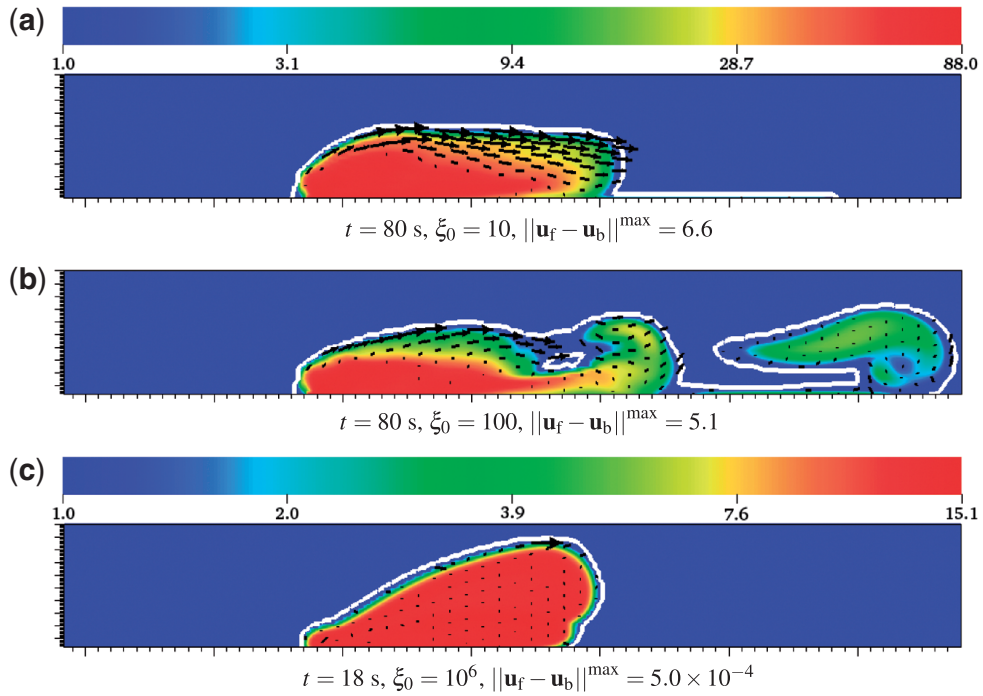

FIG. 8. Bond density z_b and relative velocity $\mathbf{u}_f - \mathbf{u}_b$ for different ξ_0. The white contour is for $\phi_b = 0.001$. Vectors in (a) and (b) have the same scale. Note the different time and bond density scale in (c).

case, the density of bound platelets ϕ_b within the thrombus is much more uniform in space (Fig. 7(c)), than for the core-shell structure seen in Fig. 7(a) and (b). The largest value of ϕ_b is close to 1, which is also the number density of unactivated platelets in the bulk flow. This result is consistent with that from the single phase model (Guy 2004a), in which all platelets and fluid are transported with a single velocity field that is divergence free. In that case, if fluid carries new platelets to a location, the existing platelets there must be carried away. Interestingly, embolization does not happen for the case with the largest drag, presumably because the thrombus is soft enough to readily deform because of fluid stresses.

The bond densities z_b and the velocity differences $\mathbf{u}_f - \mathbf{u}_b$ for the three simulations are shown in Fig. 8. Overall, the relative motion between the bound platelets and the fluid is reduced as the baseline drag is increased. For the largest baseline drag ($\xi_0 = 10^6$), the bound platelets and fluid move with approximately the same velocity, and the value of z_b is much smaller than in the simulations with smaller baseline drag. The plot of bound platelet velocity $\mathbf{u}_b$ in Fig. 9 indicates that the movement of the bound platelets is greater when the drag is increased. The bond breaking rate β as defined in Equation (2.24) is also shown in the figure. As we see from Fig. 9(a), when $\xi_0 = 10$, β is close to $\beta_0 = 0.05$, indicating that platelet bonds are stretched only a little. The largest values of β appear at the upstream end of the aggregate, which is also the location where the viscoelastic stress has its largest magnitude. With the increase of ξ_0 to 100, the largest value of β is much greater than β_0. Comparing Fig. 9(b) with Fig. 7(b) and Fig. 8(b), we see that the locations where β is largest coincide with those from which small pieces of thrombus break off. Bond breaking can be a self-reinforcing process; with a reduction of bond density in a region, each individual bond experiences larger strain and larger stress and thus is more prone to break, further reducing the bond density. For the case with $\xi_0 = 10^6$ shown in Fig. 9(c), the breaking rate β is significantly larger than β_0 throughout the thrombus, and the largest β appears at the upstream side. Because β is relatively large, the thrombus does not retain 'memory' of its earlier configurations

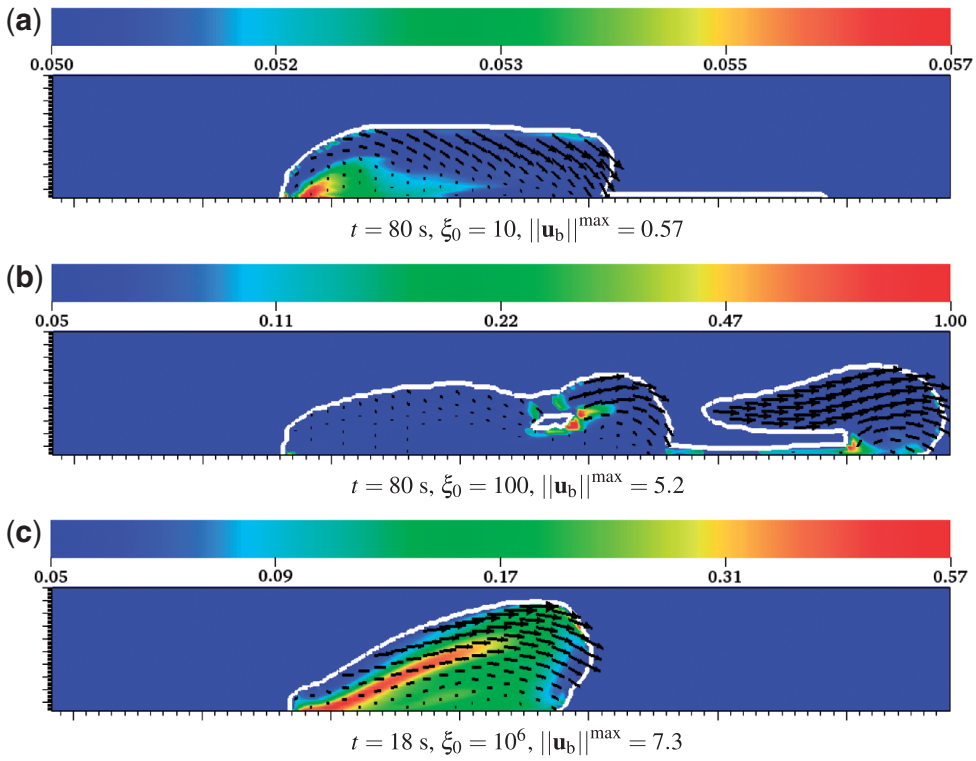

FIG. 9. Breaking rate β and bound platelet velocity $\mathbf{u}_b$ for different ξ_0. The white contour is for $\phi_b = 0.001$. Vectors in (b) and (c) have the same scale. Note the different time in (c).

and it gradually 'oozes' in the downstream direction. This behaviour increases as the thrombus rapidly grows to almost occlude the vessel, which causes the fluid velocity and shear rate to also increase rapidly. The weak thrombus (low z_b) which contains only loosely packed platelets (relatively low ϕ_b) can not hold its position and is pushed downstream by the flow. Overall, the results in this section indicate that the intraclot fluid motion may have a significant impact on the spatial structure of a forming platelet aggregate and its stability.

4.2.3 *Effects of the breaking rate function on thrombus growth* For all of the simulations presented in the previous two sections, the bound platelet generation constant C_3 in the definition of f_{ab} in Equation (2.20) was set to a relatively low value. Therefore, the average number of bonds created per platelet–platelet binding event was high. Hence, the value of n_b, the average number of bonds per bound platelet, was relatively large. Combined with small or moderate values for the breaking rate β, this implies that the rate f_{ba} at which bound platelets became unattached was always much smaller than the rate f_{ab} at which activated platelets became bound. In this section, we look at situations in which the functions f_{ab} and f_{ba} can have comparable magnitudes. The simulation results illustrate that thrombus growth can also be significantly affected by the relative speed at which bonds form and break. Here, we increase the bound platelet formation constant to $C_3 = \frac{1}{6}$ and use smaller bond formation constants, $K_{aa}^{coh} = 0.3$, $K_{ab}^{coh} = K_{bb}^{coh} = 0.015$. We also increase the parameter C_1 from 4 to 8 so that each individual bond is stiffer. Two breaking rate constants are used, $\beta_0 = 0.25$ and $\beta_0 = 3.75$. The baseline drag coefficient is set to $\xi_0 = 1$.

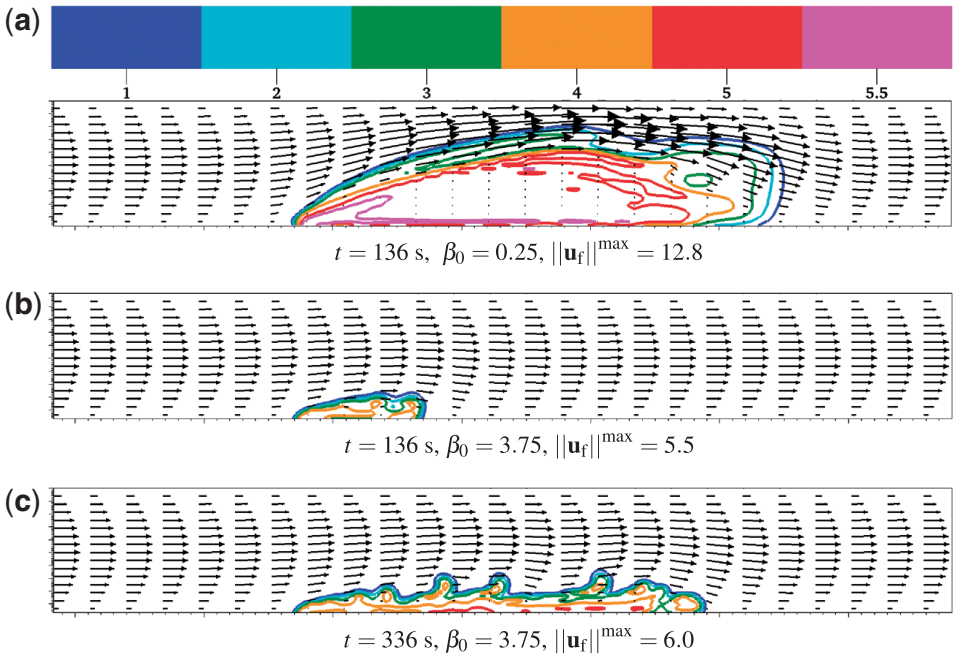

FIG. 10. Bound platelet density ϕ_b and fluid velocity $\mathbf{u}_f$ for different baseline breaking rates β_0. All vectors have the same scale.

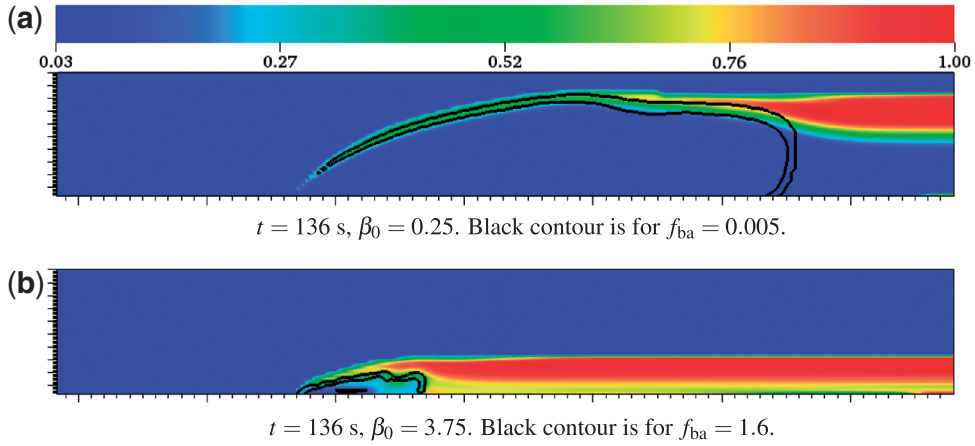

FIG. 11. The activated platelet density ϕ_a for different baseline breaking rates β_0 at $t = 136$ s.

The simulation results are shown in Figs (10) and (11). Figure 10(a) shows that the platelet aggregate can grow to occlude a large portion of the vessel when the breaking rate constant is small. In contrast, Fig. 10(b) shows that the aggregate generated with a 15-fold higher β_0 is much smaller in size and is also less dense. Figure 10(c) shows that, by a very much later time, the same aggregate has grown very little in the vertical direction and that its growth has mainly been along the bottom wall in the downstream direction. Contour plots for the largest values of the function f_{ba} and the distribution of ϕ_a are shown in Fig. 11 for the two baseline breaking rate values. For both cases, the largest f_{ba} values are located near the boundary of the thrombus. The reason for this is that when platelets first become bound near the edge of an existing aggregate and additional bonds are yet to form, there is a low average number of bonds per

bound platelet there (compared to in the interior of the aggregate). Thus, it is relatively easy for bound platelets to become unattached at the edge of the thrombus.

Comparing the situation for $\beta_0 = 3.75$ to that for $\beta_0 = 0.25$, the ratio of the unattachment rates f_{ba} is actually greater than the ratio of the β_0's. This is so because with the higher value of β_0, the average number of bonds per bound platelet, n_b is smaller. Therefore, the probability that a bond which breaks is the last one to a bound platelet, $P_1(n_{\text{b}})$ in Equation 2.23 is larger and this also contributes to make f_{ba} larger. For the situation shown in Fig. 11(a), where β_0 is small and f_{ba} is much smaller than f_{ab} in much of the thrombus, the activated platelet density ϕ_{a} is high mostly along the top edge of the thrombus. These activated platelets mainly consist of those activated near the edge of the thrombus which have not yet bound. For the situation shown in Fig. 11(b), where β_0 is large and the values of f_{ba} and f_{ab} are comparable, activated platelets are found along the entire edge of the thrombus as well in a significant portion of its interior. Among these activated platelets, especially for those near the bottom wall, a large portion comes from bound platelets that become unattached within the aggregate.

4.2.4 *Effects of shear rate on thrombus growth* In this section, we investigate the effects of shear rate on thrombus growth. Here we keep the baseline drag coefficient and bond breaking rate at $\xi_0 = 0.01$ and $\beta_0 = 0.5$. Two simulations were done with wall shear rate at 50 s^{-1} and 400 s^{-1}, respectively. Other model parameters are the same as those used in Section 4.2.2. The distribution of bound platelet density ϕ_{b} and fluid velocity $\mathbf{u}_{\text{f}}$ at different stages of the simulations are shown in Fig. 12(a–d). At the early stage

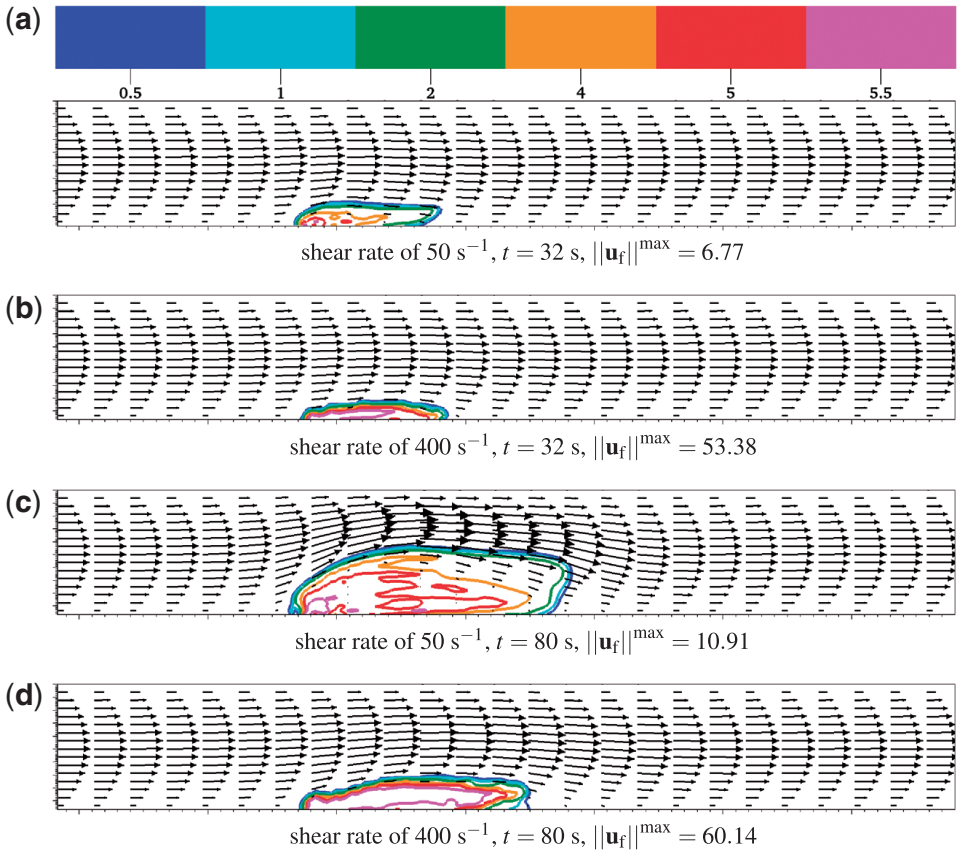

FIG. 12. Bound platelet density ϕ_b and fluid velocity $\mathbf{u}_{\text{f}}$ at different time under different shear rates.

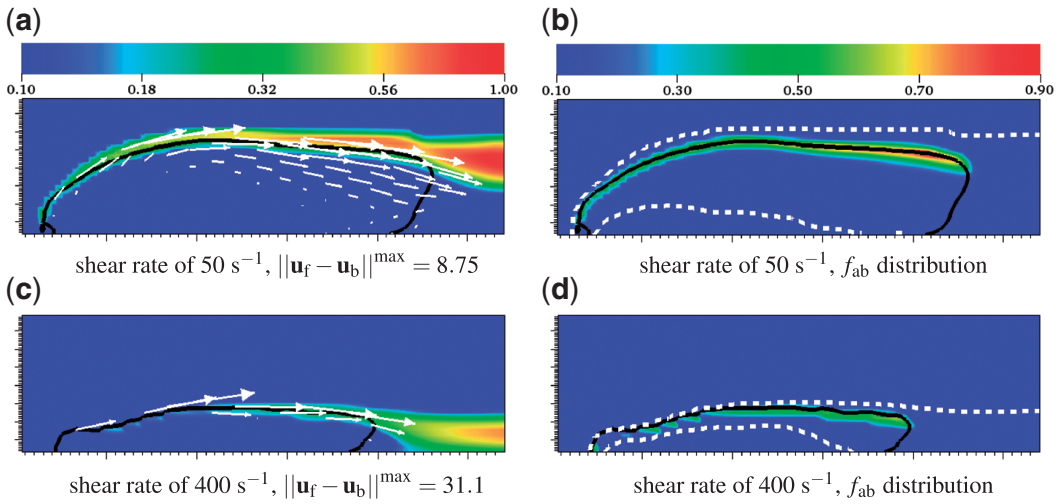

FIG. 13. All plots are for $t = 80$ s. The black contour is for $\phi_b = 1$. (a) and (c): Activated platelet density ϕ_a and relative velocity $\mathbf{u}_f - \mathbf{u}_b$. (b) and (d): Distribution of the bound platelet formation rate f_{ab}. The white dashed contour is for chemical concentration $c = 1$.

((a) and (b) for $t = 32$ s), the overall sizes of the thrombi generated under different shear rates are similar. Relative to the result with lower shear rate, thrombus in flow with higher shear rate contains a much larger region of densed packed bound platelets. Under higher shear rate, more unactivated platelets are carried into the thrombus by faster flow near the injury site. These platelets become activated and bound, causing an increase in ϕ_b. At the later stage ((c) and (d) for $t = 80$ s), the thrombus configurations from the two simulations are very different. Under the lower shear rate, the thrombus in Fig. 12(c) again exhibits the core-shell structure as seen in previous sections. For a much higher shear rate, the size of the thrombus is reduced significantly, as shown in Fig. 12(d). Dominated by a dense core, the thrombus has a much more uniform distribution of ϕ_b than that in Fig. 12(c). Close-up plots for some of the model variables are shown in Fig. 13(a-d). Comparing Fig. 13(a) with (c), it can be seen that with the increase in shear rate, the amount of activated platelets above the thrombus edge is reduced dramatically. With low shear rate and slow-moving background flow, unactivated platelets near the thrombus may have enough time to get activated and attached to the thrombus. When the shear rate is high, both the activating chemical and unbound platelets are washed downstream away from the existing thrombus by fast flow. As the result, the rate at which platelets become bound (function f_{ab}) is higher under lower shear rate. This is illustrated in Fig. 13(b) and (d).

5. Conclusion

We have developed a two-phase continuum model for platelet thrombosis in a blood vessel the size of a coronary artery. In the model, activated platelets aggregate through the formation of interplatelet bonds. The platelet aggregate is treated as a viscoelastic material whose material parameters (e.g. elastic modulus) vary in space and time and evolve as the number density of platelets in the aggregate and the number density of the elastic bonds holding them together change. The bulk blood is treated as a viscous Newtonian fluid. The model consists of a system of advection–diffusion–reaction equations (for the number densities of three platelet populations, the concentration of an activating chemical and the number density of platelet bonds), coupled sets of momentum equations for the velocity fields of the bound platelets and the bulk blood, a volume-averaged incompressibility constraint, and a constitutive

equation for the viscoelastic stresses produced by platelet bonds. A critical feature of the model is that the bound platelets within a growing thrombus move in a velocity field different from that for the bulk fluid. The relative motion of the two materials produces an interphase frictional drag, whose magnitude changes with the number density of platelets in the thrombus, that acts on both the bound platelets and the bulk fluid.

Our model is a major extension of the single-phase continuum model developed in Fogelson (1992) and Fogelson & Guy (2004). A limitation of that model is that it does not allow relative motion of the platelets and fluid. This has two important consequences. 1) For a thrombus to form, it must do so much more rapidly than occurs physiologically and 2) The number density of platelets within an aggregate can be only slightly higher (via diffusive motion) than the number density of non-activated platelets in the blood. In contrast, in real thrombi, the platelet number density can be more than 100-fold greater than the number density of platelets in the bulk blood. The two-phase model was developed to overcome these limitations of the single-phase model.

Compared with other models of thrombus development, our model has several advantages for studying platelet thrombosis in vessels whose diameter has a millimetre scale such as the coronary arteries. Most existing models (e.g. those in Flamm & Diamond 2012; Xu *et al.* (2008)) track the movement and interactions of individual platelets and thus are well suited to describe thrombus development in small vessels and microfluidic devices. Because of the very large number of platelets which interact during arterial thrombus formation, these models are not suitable for studying it. In contrast, within our continuum model, the different types of platelets and their distributions are represented by number densities. Additionally, the spatial scale of the model is that of the vessel itself. Thus the model is suitable to study platelet thrombosis in large arteries. But our model does not ignore processes at the scale of individual platelets. In fact, it was derived from a two-phase model that explicitly treats both the vessel and individual platelet spatial scales. Important aspects of the small-scale are captured through appropriate closure approximations made in going from the two-scale model to the vessel-scale one.

The new model should also be compared to the continuum model described in Leiderman & Fogelson (2011) and Leiderman & Fogelson (2013). That model is for the combined processes of platelet accumulation and coagulation under flow. In it, the growing platelet thrombus is treated as a porous solid made up of stationary and permanently bound platelets through which the fluid and unbound platelets can move. The permeability of the thrombus decreases as the density of bound platelets increases. This is similar to our assumption here that the interphase drag grows with the bound platelet number density. The model in Leiderman & Fogelson (2011) and Leiderman & Fogelson (2013) includes more biology than the one we propose here in that it includes the coagulation reaction system. On the other hand, it cannot be used to study the mechanics of bound platelet aggregates, including the possibility that the thrombus can break up when subject to large stresses by the flow. The new two-phase model, which treats the thrombus as a viscoelastic material with evolving extent and material properties, was specifically formulated for such purposes. The generation and breakup of interplatelet bonds, the magnitude and distribution of the viscoelastic stresses within the thrombus, and the movement and embolization of portions of it, are all closely coupled with the hydrodynamic properties of the background flow. For example, the thrombus can respond strongly to especially high shear stresses transmitted to it via the interphase drag force. Both the model in Leiderman & Fogelson (2011) and Leiderman & Fogelson (2013) and that in the current paper can capture the effects on clot development of intraclot transport of fluid and platelets, and the role that limitations in intraclot transport at high bound platelet densities might have in slowing further thrombus growth. Variations in intraclot transport at different stages of thrombus development is increasingly recognized as an important regulator of the process (Stalker *et al.* 2014; Tomaiuolo *et al.* 2014; Welsh *et al.* 2014).

While the main contribution of this article is the introduction of a two-phase model of platelet aggregation that allows relative motion between the bound platelets and the bulk fluid, two other modelling innovations are noteworthy. One is the introduction of a way of incorporating the unbinding of a platelet from a thrombus in a continuum model that does not explicitly track the bonds from each bound platelet. The basis of the approach is to assume that, at each location, the bonds are distributed among bound platelets with a Poisson-like distribution. The other is incorporating stresses due to interplatelet bonds with non-zero rest length. To do this, we exploited our previously-introduced expression for the local mean squared bond length (Fogelson & Guy, 2004).

As described here, the new model allows for platelet activation by exposure to a soluble chemical agonist released by other platelets at the time they become activated. This is the mode of action of adenosine diphosphate which is secreted from a platelet's storage granules when that platelet is activated (Andrews, & Berndt 2004). Other important platelet activation mechanisms can be readily added to the model framework. These include the ongoing production of the enzyme thrombin on the surfaces of activated platelets, its release into the plasma, and activation of other platelets after binding to their thrombin receptors (Andrews, & Berndt 2004). They also include activation, mediated by one of several families of platelet receptors, upon a platelet's contact with the injured vascular wall (Jackson 2007; Ruggeri 2009; Broos *et al.* 2011; Kasirer-Friede *et al.* 2014), or through its experience of high shear stresses (Moake *et al.* 1986). The model can also be adapted to treat transient aggregation of non-activated platelets in the presence of very large shear gradients (Nesbitt *et al.* 2009).

The numerical results presented in this article are intended to illustrate the capabilities of the new two-phase model. A number of simulations are shown in which platelet activation and accumulation begins in a small 'injury zone'. We showed the temporal evolution of the model's variables during development of a thrombus for a low baseline drag coefficient ξ_0. This showed the interplay among transport of the different platelet and chemical species, the activation of platelets, the formation and breaking of interplatelet bonds and the development of the viscoelastic stresses produced by those bonds when their lengths differ from their equilibrium length. We saw that the model naturally produces a thrombus with a dense core and a looser shell, as seen in recent experiments (Stalker *et al.* 2014). The computed bound platelet density ϕ_b in the core was several-fold higher than the unactivated platelet density in the bulk blood. When using a smaller value for the platelet volume v_p, ϕ_b reaches higher values, over a longer period of time; its ultimate value is limited by the shut-down of intraclot platelet transport when the drag becomes very large as $\theta_b = v_p\phi_\mathrm{b}$ approaches $\theta_\mathrm{b}^{\max}$.

We note that the core-shell structure reported in Stalker *et al.* (2014) and similar observations reported in van Gestel *et al.* (2002) pertain to haemostatic clots produced by puncturing the blood vessel wall and involve blood flow into the extravascular space. To our knowledge, it is not known whether similar structures appear in thrombotic clots growing into the vessel lumen. In our simulations, the 'shell' seems to be a transient structure which can either be torn off by fluid stresses or become part of the core as the density of bound platelets in it becomes sufficiently high.

In a set of simulations with different baseline drag coefficients (ξ_0), we saw development of thrombi of different size, density and stability. In one case, a stable thrombus with dense core and loose shell developed. For higher drag, the shell structure repeatedly was torn off of the thrombus and then reformed. For the highest drag coefficient, a low density thrombus with weak elasticity developed. While it occupied much of the vessel lumen, the fluid flow within the thrombus was reduced only a little because the weak viscoelasticity allowed the thrombus to 'ooze' in response to the drag forces. In a pair of simulations with different baseline bond breaking rates (β_0), we see that the relative rates of platelet attachment to and detachment from a thrombus can have profound effects on the resulting thrombus shape.

We are in the process of conducting systematic studies of the new model with parameters reflective of pathological conditions. Results from these studies will be reported in a separate publication. The model presented here is also intended to be the foundation for a model including detailed platelet-injury interactions, other modes of platelet activation, and eventually coagulation and fibrin formation with which we can explore thrombus formation on ruptured atherosclerotic plaques.

Funding

This work was supported in part by NSF grant DMS-1160432.

References

ANAND, M., RAJAGOPAL, K. & RAJAGOPAL, K. (2005) A model for the formation and lysis of blood clots. *Pathophysiol. Haemost. Thromb.*, **34**, 109–120.

ANDREWS, R. K. & BERNDT, M. C. (2004) Platelet physiology and thrombosis. *Thromb. Res.*, **114**, 447–473.

BRASS, L. F., WANNEMACHER, K. M., MA, P. & STALKER, T. J. (2011) Regulating thrombus growth and stability to achieve optimal response to injury. *J. Thromb. Hemost.*, **9**, 66–75.

BROOS, K., FEYS, H. B., DEMEYER, S. F. VANHOORELBEKE, K. & DECKMYN, H. (2011) Platelets at work in primary hemostasis, *Blood Rev.*, **25**, 155–167.

COLELLA, P. (1990) Multidimesional upwind methods for hyperbolic conservation laws. *J. Comput. Phys.*, **87**, 171–200.

DU, J., GUY, R. D., FOGELSON, A. L., WRIGHT, G. B. & KEENER, J. P. (2013) An interface-capturing regularization method for solving the equations for two-fluid mixtures. *Commun. Comput. Phys.*, **14**, 1322–1346.

FLAMM, M. H. & DIAMOND, S. L. (2012) Multiscale systems biology and physics of thrombosis under flow. *Ann. Biomed. Eng.*, **40**, 2355–2364.

FOGELSON, A. L. (1984) A mathematical model and numerical method for studying platelet adhesion and aggregation during blood clotting. *J. Comput. Phys.*, **56**, 111–134.

FOGELSON, A. L. (1992) Continuum models of platelet aggregation: formulation and mechanical properties. *SIAM JAM*, **52**, 1089–1110.

FOGELSON, A. L. (1993) Continuum Models of Platelet Aggregation: Mechanical Properties and Chemically-induced Phase Transitions. *Contemp. Math.*, **141**, 279–294.

FOGELSON, A. L. & GUY, R. D. (2004) Platelet-wall interactions in continuum models of platelet aggregation:formulation and numerical solution. *Math. Med. Biol.*, **21**, 293–334.

FOGELSON, A. L. & GUY, R. D. (2008) Immersed-boundary-type models of intravascular platelet aggregation. *Comput. Methods Appl. Mech. Eng.*, **197**, 2087–2104.

FOGELSON, A. L., HUSSAIN, Y. H. & LEIDERMAN, K. (2012) Blood clot formation under flow: The importance of factor XI depends strongly on platelet count. *Biophys. J.*, **102**, 10–18.

FOGELSON, A. L. & KEENER, J. P. (2010) Toward an understanding of fibrin branching structure. *Phys. Rev. E.*, **81**, 051922.

FOGELSON, A. L. & NEEVES, K. B. (2015) Fluid Mechanics of Blood Clotting. *Annu. Rev. Fluid Mech.*, **47**, 377–403.

FOGELSON, A. L. & TANIA, N. (2005) Coagulation under flow: The influence of flow-mediated transport on the initiation and inhibition of coagulation. *Pathophysiol. Haemost. Thromb.*, **34**, 91–108.

GUY, R. D. (2004a) Continuum models of platelet aggregation: closure models, computational methods, and simulation. Ph.D. *Thesis*, University of Utah, Salt Lake City, Utah, 84112 USA.

GUY, R. D. (2004b) Asymptotic analysis of PTT type closures for network models with variable junction concentrations. *J. Non-Newtonian Fluid Mech.*, **123**, 223–235.

GUY, R. D. & FOGELSON, A. L. (2007) Modeling fibrin gel formation in a shear flow. *Math. Med. Biol.*, **24**, 111–130.

JACKSON, S. P. (2007) The growing complexity of platelet aggregation. *Blood*, **109**, 5087–5095.

KASIRER-FRIEDE, A., KAHN, M. L., & SHATTIL, S. J. (2014) Platelet integrins and immunoreceptors. *Immunol. Rev.*, **218**, 247–264.

KUHARSKY, A. L. & FOGELSON, A. L. (2001) Surface-mediated control of blood coagulation: the role of binding site densities and platelet deposition. *Biophys. J.*, **80**, 1050–1074.

LEIDERMAN, K. & FOGELSON, A. L. (2011) Grow with the flow: a spatial-temporal model of platelet deposition and blood coagulation under flow. *Math. Med. Biol.*, **28**, 47–84.

LEIDERMAN, K. & FOGELSON, A. L. (2013) The influence of hindered transport on the development of platelet thrombi under flow. *Bull. Math. Biol.*, **75**, 1255–1283.

MOAKE, J. L., TURNER, N. A., STATHOPOULOS, N. A., NOLASCO, L. H. & HELLUMS, J. D. (1986) Involvement of large plasma von Willebrand factor (vWF) multimers and unusually large vWF forms derived from endothelial cells in shear stress-induced platelet aggregation. *J. Clin. Investig.*, **78**, 1456–1461.

NESBITT, W. S., WESTEIN, E., TOVAR-LOPEZ, F. J., TOLOUEI, E., MITCHELL, A., FU, J., CARBERRY, J., FOURAS, A. & JACKSON, S. P. (2009) A shear gradientdependent platelet aggregation mechanism drives thrombus formation. *Nature Med.*, **15**, 665–673.

RUGGERI, Z. M. (2009) Platelet adhesion under flow. *Microcirculation*, **16**, 58–83.

STALKER, T. J., TRAXLER, E. A., WU, J., WANNEMACHER, K. M., CERMIGNANO, S. L., VORONOV, R., DIAMOND, S. L. & BRASS, L. F. (2013) Hierarchical organization in the hemostatic response and its relationship to the platelet-signaling network. *Blood*, **121**, 1875–1885.

STALKER, T. J., WELSH, J. D., TOMAIUOLO, M., WU, J., COLACE, T. V., DIAMOND, S. L. & BRASS, L. F. (2014) A systems approach to hemostasis: 3. Thrombus consolidation regulates intrathrombus solute transport and local thrombin activity. *Blood*, **124**, 1824–1831.

STORTI, F. & VAN DE VOSSE, F. N. (2014) A continuum model for platelet plug formation, growth, and deformation, *Int. J. Numer. Method. Biomed. Eng.*, **30**, 1541–1557.

STORTI, F., VAN KEMPEN, T. H. S. & VAN DE VOSSE, F. N. (2014) A continuum model for platelet plug formation and growth, *Int. J. Numer. Method. Biomed. Eng.*, **30**, 634–658.

TANNER, R. I. (2000) *Engineering Rheology.* London: Oxford University Press.

TOMAIUOLO, M., STALKER, T. J., WELSH, J. D., DIAMOND, S. L., SINNO, T. & BRASS, L. F. (2014) A systems approach to hemostasis: 2. Computational analysis of molecular transport in the thrombus microenvironment. *Blood*, **124**, 1816–1823.

TOKAREV, A., SIRAKOV, I., PANASENKO, G., VOLPERT, V., SHNOL, E., BUTYLIN, A. & ATAULLAKHANOV, F. (2012) A continuous mathematical model of platelet thrombus formation in blood flow. *Russian J. Numer. Anal. Math. Modeling*, **27**, 191–212.

VAN GESTEL, M. A., HEEMSKERK, J. W. H., SLAAF, D. W., HEIJNEN, V. V. T., SAGE, S. O., RENEMAN, R. S. & OUDE EGBRINK, M. G. A. (2002) Real-Time Detection of Activation Patterns in Individual Platelets during Thromboembolism in vivo: Differences between Thrombus Growth and Embolus Formation. *Journal of Vascular Research*, **39**, 534–543.

WANG, N. T. & FOGELSON, A. L. (1999) Computational methods for continuum models of platelet aggregation. *J. Comput. Phys.*, **151**, 649–675.

WELLER, F. (2010) A free boundary problem modeling thrombus growth. *J. Math. Biol.*, **61**, 805–818.

WELSH, J. D., STALKER, T. J., VORONOV, R., MUTHARD, R. W., TOMAIUOLO, M., DIAMOND, S. L. & BRASS, L. F. (2014) A systems approach to hemostasis: 1. The interdependence of thrombus architecture and agonist movements in the gaps between platelets. *Blood*, **124**, 1808–1815.

WRIGHT, G. B., GUY, R. D., DU, J. & FOGELSON, A. L. (2011) A high-resolution finite-difference method for simulating two-fluid, viscoelastic gel dynamics. *J. Non-Newtonian Fluid Mech.*, **166**, 1137–1157.

WRIGHT, G. B., GUY, R. D. & FOGELSON, A. L. (2008) An efficient and robust method for simulating two-phase gel dynamics. *SIAM J. Sci. Comput.*, **30**, 2535–2565.

WUFSUS, A. R., MACERA, N. E. & NEEVES, K. B. (2013) The hydraulic permeability of blood clots as a function of fibrin and platelet density. *Biophys. J.*, **104**, 1812–1823.

XU, Z., CHEN, N., KAMOCKA, M., ROSEN, E. & ALBER, M. (2008) A multiscale model of thrombus development. *J. R. Soc. Interface*, **5**, 705–722.

Appendix

Here we sketch the derivation of Equations 2.14 and 2.15 from a model that involves two spatial scales, one the scale of a platelet and the other the scale of the vessel in which the thrombus is forming. We are interested in the case that the ratio ϵ of these length scales is very small; the equations we derive hold at leading order in ϵ.

Define $\tilde{E}(\mathbf{x}, \mathbf{r}, t)$ so that $\tilde{E}(\mathbf{x}, \mathbf{r}, t)d\mathbf{r}$ is the concentration of elastic bonds between bound platelets at $\mathbf{x}$ and in a small volume $d\mathbf{r}$ around $\mathbf{x} + \mathbf{r}$. Below, we make the change of variables $\mathbf{r} = \epsilon\mathbf{y}$, $E(\mathbf{x}, \mathbf{y}, t) = \epsilon^3\tilde{E}(\mathbf{x}, \mathbf{r}, t)$, and we introduce the quantities z_b and $\underline{\underline{\sigma}}^\mathrm{b}$ defined by:

$$z_\mathrm{b}(\mathbf{x}, t) = \int_{\mathbf{r}} \tilde{E}(\mathbf{x}, \mathbf{r}, t)d\mathbf{r} = \int_{\mathbf{y}} E(\mathbf{x}, \mathbf{y}, t)d\mathbf{y}, \tag{A.1}$$

$$\underline{\underline{\sigma}}^\mathrm{b}(\mathbf{x}, t) = \tfrac{1}{2}\int_{\mathbf{y}} E(\mathbf{x}, \mathbf{y}, t)S(|\mathbf{y}|)\mathbf{y}\mathbf{y}^T d\mathbf{y}, \tag{A.2}$$

where $S(|\mathbf{y}|)$ represents the stiffness of the bond as a function of the length of the bond. From these definitions, we see that z_b is the density of bonds eminating from bound platelets at location $\mathbf{x}$ and the components of $\underline{\underline{\sigma}}^\mathrm{b}$ are the stresses produced by those bonds.

The derivations of evolution equations for E, $\underline{\underline{\sigma}}^\mathrm{b}$, and z_b that follow are similar to those given in our previous papers (Fogelson, 1992; Fogelson & Guy, 2004), but differ in that in the two-phase model, the velocity field need not be incompressible. Hence, certain terms in the derivation that vanished in the incompressible case remain in the equations.

A.1 *Evolution equation for E*

Toward the goal of deriving an evolution equation for E and, using it, to derive evolution equations for z_b and $\underline{\underline{\sigma}}^\mathrm{b}$, let $\Omega_x(t)$ and $\Omega_\xi(t)$ be two material regions of fluid, and define $N(t)$ by

$$N(t) = \int_{\Omega_x(t)}\int_{\Omega_\xi(t)} \tilde{E}(\mathbf{x}, \boldsymbol{\xi} - \mathbf{x}, t)d\boldsymbol{\xi}d\mathbf{x}. \tag{A.3}$$

$N(t)$ is the number of bonds between bound platelets in $\Omega_x(t)$ and $\Omega_\xi(t)$. We assume that the number of bonds between platelets in these material regions changes only through the formation and breaking of bonds, i.e.

$$\frac{dN}{dt} = \int_{\Omega_x(t)}\int_{\Omega_\xi(t)} \left\{\tilde{\alpha}\big(|\mathbf{x} - \boldsymbol{\xi}|, \phi_\mathrm{a}(\mathbf{x}, t), \phi_\mathrm{a}(\boldsymbol{\xi}, t), \phi_\mathrm{b}(\mathbf{x}, t), \phi_\mathrm{b}(\boldsymbol{\xi}, t)\big) - \tilde{\beta}(|\boldsymbol{\xi} - \mathbf{x}|)\tilde{E}(\mathbf{x}, \boldsymbol{\xi} - \mathbf{x}, t)\right\} d\mathbf{x}d\boldsymbol{\xi}, \tag{A.4}$$

where we have introduced the short-hand notation

$$\begin{aligned}\tilde{\alpha}\big(|\mathbf{x} - \boldsymbol{\xi}|, \phi_\mathrm{a}(\mathbf{x}, t), \phi_\mathrm{a}(\boldsymbol{\xi}, t), \phi_\mathrm{b}(\mathbf{x}, t), \phi_\mathrm{b}(\boldsymbol{\xi}, t)\big) \equiv\ & \tilde{\alpha}^{coh}_{aa}(|\mathbf{x} - \boldsymbol{\xi}|)\phi_\mathrm{a}(\mathbf{x}, t)\phi_\mathrm{a}(\boldsymbol{\xi}, t) \\ & + \tilde{\alpha}^{coh}_{ab}(|\mathbf{x} - \boldsymbol{\xi}|)\big(\phi_\mathrm{a}(\mathbf{x}, t)\phi_\mathrm{b}(\boldsymbol{\xi}, t) + \phi_\mathrm{a}(\boldsymbol{\xi}, t)\phi_\mathrm{b}(\mathbf{x}, t)\big) \\ & + \tilde{\alpha}^{coh}_{bb}(|\mathbf{x} - \boldsymbol{\xi}|)\phi_\mathrm{b}(\mathbf{x}, t)\phi_\mathrm{b}(\boldsymbol{\xi}, t)\end{aligned} \tag{A.5}$$

for the rate of bond formation between platelets at $\mathbf{x}$ and platelets at $\boldsymbol{\xi}$.

Next, we compute $\frac{dN}{dt}$ using (A.3). To facilitate this calculation, we convert the integrals over $\Omega_x(t)$ and $\Omega_\xi(t)$ to ones over the preimages of these point sets, $\Omega_x(0)$ and $\Omega_\xi(0)$, respectively, under the flow map $\mathbf{x}(t) = \phi(t;\mathbf{x_0})$ and $\boldsymbol{\xi}(t) = \phi(t;\xi_0)$:

$$N(t) = \int_{\Omega_x(0)} \int_{\Omega_\xi(0)} \tilde{E}(\mathbf{x}(t;\mathbf{x_0}), \boldsymbol{\xi}(t;\xi_0) - \mathbf{x}(t,\mathbf{x_0}), t) J(t;\mathbf{x_0}) J(t;\xi_0) d\xi_0 d\mathbf{x_0}. \tag{A.6}$$

Here, $J(t;\mathbf{x_0})$ and $J(t;\xi_0)$ are the Jacobian determinants of the flow maps $\mathbf{x}(t) = \phi(t;\mathbf{x_0})$ and $\boldsymbol{\xi}(t) = \phi(t;\xi_0)$, respectively. Denoting by $\nabla_1\tilde{E}$ and $\nabla_2\tilde{E}$ the gradients of $\tilde{E}$ with respect to its first and second vector arguments, respectively, we find that

$$\begin{aligned}\frac{dN(t)}{dt} = \int_{\Omega_x(0)} \int_{\Omega_\xi(0)} \Big[\Big\{ &\frac{\partial \tilde{E}}{\partial t} + \frac{d\mathbf{x}}{dt}(t;\mathbf{x_0}) \cdot \nabla_1 \tilde{E}\big(\mathbf{x}(t;\mathbf{x_0}), \boldsymbol{\xi}(t;\xi_0) - \mathbf{x}(t;\mathbf{x_0}), t\big) \\ &+ \Big(\frac{d\boldsymbol{\xi}}{dt}(t;\xi_0) - \frac{d\mathbf{x}}{dt}(t;\mathbf{x_0})\Big) \cdot \nabla_2 \tilde{E}\big(\mathbf{x}(t;\mathbf{x_0}), \boldsymbol{\xi}(t;\xi_0) - \mathbf{x}(t;\mathbf{x_0}), t\big)\Big\} J(t;\mathbf{x_0}) J(t;\xi_0) \\ &+ \Big\{ \tilde{E} J_t(t;\mathbf{x_0}) J(t;\xi_0) + \tilde{E} J(t;\mathbf{x_0}) J_t(t;\xi_0) \Big\} \Big] d\xi_0 d\mathbf{x_0}.\end{aligned} \tag{A.7}$$

Recalling that $\frac{d\mathbf{x}}{dt}(t;\mathbf{x_0}) = \mathbf{u}_\mathrm{b}(\mathbf{x}(t;\mathbf{x_0}), t)$, $\frac{d\boldsymbol{\xi}}{dt}(t;\xi_0) = \mathbf{u}_\mathrm{b}(\boldsymbol{\xi}(t;\xi_0), t)$, $\frac{\partial J(t;\mathbf{x_0})}{\partial t} = J(t;\mathbf{x_0}) \nabla \cdot \mathbf{u}_\mathrm{b}(\mathbf{x}(t;\mathbf{x_0}), t)$, and $\frac{\partial J(t;\xi_0)}{\partial t} = J(t;\xi_0) \nabla \cdot \mathbf{u}_\mathrm{b}(\xi(t;\xi_0), t)$, Equation (A.7) becomes

$$\begin{aligned}\frac{dN(t)}{dt} = \int_{\Omega_x(0)} \int_{\Omega_\xi(0)} \Big\{ &\frac{\partial \tilde{E}}{\partial t} + \frac{d\mathbf{x}}{dt}(t;\mathbf{x_0}) \cdot \nabla_1 \tilde{E}\big(\mathbf{x}(t;\mathbf{x_0}), \boldsymbol{\xi}(t;\xi_0) - \mathbf{x}(t;\mathbf{x_0}), t\big) \\ &+ \Big(\frac{d\boldsymbol{\xi}}{dt}(t;\xi_0) - \frac{d\mathbf{x}}{dt}(t;\mathbf{x_0})\Big) \cdot \nabla_2 \tilde{E}\big(\mathbf{x}(t;\mathbf{x_0}), \boldsymbol{\xi}(t;\xi_0) - \mathbf{x}(t;\mathbf{x_0}), t\big) \\ &+ \tilde{E}\, \nabla \cdot \mathbf{u}_\mathrm{b}(\mathbf{x}(t;\mathbf{x_0}), t) + \tilde{E}\, \nabla \cdot \mathbf{u}_\mathrm{b}(\boldsymbol{\xi}(t;\xi_0), t) \Big\} J(t;\mathbf{x_0}) J(t;\xi_0) d\xi_0 d\mathbf{x_0}.\end{aligned} \tag{A.8}$$

Returning to our original variables,

$$\begin{aligned}\frac{dN(t)}{dt} = \int_{\Omega_x(t)} \int_{\Omega_\xi(t)} \Big[\Big\{ &\tilde{E}_t(\mathbf{x}, \boldsymbol{\xi} - \mathbf{x}, t) + \mathbf{u}_\mathrm{b}(\mathbf{x}, t) \cdot \nabla_1 \tilde{E}\big(\mathbf{x}, \boldsymbol{\xi} - \mathbf{x}, t\big) \\ &+ \Big(\mathbf{u}_\mathrm{b}(\boldsymbol{\xi}, t) - \mathbf{u}_\mathrm{b}(\mathbf{x}, t)\Big) \cdot \nabla_2 \tilde{E}\big(\mathbf{x}, \boldsymbol{\xi} - \mathbf{x}, t\big) \\ &+ \tilde{E}(\mathbf{x}, \boldsymbol{\xi} - \mathbf{x}, t)\, \nabla \cdot \mathbf{u}_\mathrm{b}(\mathbf{x}, t) + \tilde{E}(\mathbf{x}, \boldsymbol{\xi} - \mathbf{x}, t)\, \nabla \cdot \mathbf{u}_\mathrm{b}(\boldsymbol{\xi}, t) \Big] d\boldsymbol{\xi} d\mathbf{x}.\end{aligned} \tag{A.9}$$

Making use of this in Equation (A.4) and the arbitrariness of the regions of integration, we obtain,

$$\begin{aligned}&\tilde{E}_t(\mathbf{x}, \boldsymbol{\xi} - \mathbf{x}, t) + \mathbf{u}_\mathrm{b}(\mathbf{x}, t) \cdot \nabla_1 \tilde{E}\big(\mathbf{x}, \boldsymbol{\xi} - \mathbf{x}, t\big) + \Big(\mathbf{u}_\mathrm{b}(\boldsymbol{\xi}, t) - \mathbf{u}_\mathrm{b}(\mathbf{x}, t)\Big) \cdot \nabla_2 \tilde{E}\big(\mathbf{x}, \boldsymbol{\xi} - \mathbf{x}, t\big) \\ &\quad + \tilde{E}(\mathbf{x}, \boldsymbol{\xi} - \mathbf{x}, t)\, \nabla \cdot \mathbf{u}_\mathrm{b}(\mathbf{x}, t) + \tilde{E}(\mathbf{x}, \boldsymbol{\xi} - \mathbf{x}, t)\, \nabla \cdot \mathbf{u}_\mathrm{b}(\boldsymbol{\xi}, t) \\ &\quad = \tilde{\alpha}\big(|\mathbf{x} - \boldsymbol{\xi}|, \phi_\mathrm{a}(\mathbf{x}, t), \phi_\mathrm{a}(\boldsymbol{\xi}, t), \phi_\mathrm{b}(\mathbf{x}, t), \phi_\mathrm{b}(\boldsymbol{\xi}, t)\big) - \tilde{\beta}(|\boldsymbol{\xi} - \mathbf{x}|) \tilde{E}(\mathbf{x}, \boldsymbol{\xi} - \mathbf{x}, t).\end{aligned} \tag{A.10}$$

Letting $\boldsymbol{\xi} - \mathbf{x} = \epsilon\mathbf{y}$, $\alpha(|\mathbf{y}|, \phi_{\mathrm{a}}(\mathbf{x},t)\phi_{\mathrm{a}}(\mathbf{x}+\epsilon\mathbf{y},t), \phi_{\mathrm{b}}(\mathbf{x},t), \phi_{\mathrm{b}}(\mathbf{x}+\epsilon\mathbf{y},t)) = \epsilon^3\tilde{\alpha}\big(|\mathbf{x}-\boldsymbol{\xi}|, \phi_{\mathrm{a}}(\mathbf{x},t), \phi_{\mathrm{a}}(\boldsymbol{\xi},t), \phi_{\mathrm{b}}(\mathbf{x},t), \phi_{\mathrm{b}}(\boldsymbol{\xi},t)\big)$, $\beta(|\mathbf{y}|) = \tilde{\beta}(|\boldsymbol{\xi}-\mathbf{x}|)$, and $E(\mathbf{x},\mathbf{y},t) = \epsilon^3\tilde{E}(\mathbf{x},\boldsymbol{\xi}-\mathbf{x},t)$, we obtain

$$\begin{aligned} &E_t(\mathbf{x},\mathbf{y},t) + \mathbf{u}_{\mathrm{b}}(\mathbf{x},t)\cdot\nabla_x E\big(\mathbf{x},\mathbf{y},t\big) + \Big(\mathbf{u}_{\mathrm{b}}(\mathbf{x}+\epsilon\mathbf{y},t) - \mathbf{u}_{\mathrm{b}}(\mathbf{x},t)\Big)\cdot\frac{1}{\epsilon}\nabla_y E\big(\mathbf{x},\mathbf{y},t\big) \\ &\quad + E(\mathbf{x},\mathbf{y},t)\,\nabla\cdot\mathbf{u}_{\mathrm{b}}(\mathbf{x},t) + E(\mathbf{x},\mathbf{y},t)\,\nabla\cdot\mathbf{u}_{\mathrm{b}}(\mathbf{x}+\epsilon\mathbf{y},t) \\ &= \alpha(|\mathbf{y}|, \phi_{\mathrm{a}}(\mathbf{x},t)\phi_{\mathrm{a}}(\mathbf{x}+\epsilon\mathbf{y},t), \phi_{\mathrm{b}}(\mathbf{x},t), \phi_{\mathrm{b}}(\mathbf{x}+\epsilon\mathbf{y},t)) - \beta(|\mathbf{y}|)E(\mathbf{x},\mathbf{y},t). \end{aligned} \tag{A.11}$$

Expanding $\mathbf{u}_{\mathrm{b}}(\mathbf{x}+\epsilon\mathbf{y},t)$, $\phi_{\mathrm{a}}(\mathbf{x}+\epsilon\mathbf{y},t)$, and $\phi_{\mathrm{b}}(\mathbf{x}+\epsilon\mathbf{y},t)$ about $(\mathbf{x},t)$, using these expansions in Equation (A.12), keeping only the leading order terms in ϵ, and using Equation (A.5), we obtain

$$\begin{aligned} &E_t + \nabla_x\cdot(\mathbf{u}_{\mathrm{b}}E) + (\mathbf{y}\cdot\nabla\mathbf{u}_{\mathrm{b}}(\mathbf{x},t))\cdot\nabla_y E) + E\,\nabla\cdot\mathbf{u}_{\mathrm{b}} \\ &= \alpha_{aa}^{coh}(|\mathbf{y}|)\phi_{\mathrm{a}}(\mathbf{x},t)^2 + 2\alpha_{ab}^{coh}(|\mathbf{y}|)\phi_{\mathrm{a}}(\mathbf{x},t)\phi_{\mathrm{b}}(\mathbf{x},t) + \alpha_{bb}^{coh}(|\mathbf{y}|)\phi_{\mathrm{b}}(\mathbf{x},t)^2 - \beta(|\mathbf{y}|)E. \end{aligned} \tag{A.12}$$

This equation differs from the corresponding one in our single-phase model in three ways: the term $\nabla_x\cdot(\mathbf{u}_{\mathrm{b}}E)$ here would be replaced by $\mathbf{u}\cdot\nabla E$, the term $E\nabla\cdot\mathbf{u}_{\mathrm{b}}$ here would be absent, and the term $\alpha_{aa}^{coh}(|\mathbf{y}|)\phi_{\mathrm{a}}(\mathbf{x},t)^2 + 2\alpha_{ab}^{coh}(|\mathbf{y}|)\phi_{\mathrm{a}}(\mathbf{x},t)\phi_{\mathrm{b}}(\mathbf{x},t) + \alpha_{bb}^{coh}(|\mathbf{y}|)\phi_{\mathrm{b}}(\mathbf{x},t)^2$ here would be replaced by $\alpha^{coh}(|\mathbf{y}|)\phi_{\mathrm{a}}(\mathbf{x},t)^2$.

A.2 *Equations for* $\underline{\underline{\sigma}}^{\mathrm{b}}(\mathbf{x},t)$ *and* $z_{\mathrm{b}}(\mathbf{x},t)$

We specialize to the case that the bond stiffness function $S(|\mathbf{y}|) = S_0(1-\frac{R}{|\mathbf{y}|})$, where the stiffness S_0 and rest length R are positive and nonnegative, respectively. Let

$$\underline{\underline{\sigma}}_0^{\mathrm{b}}(\mathbf{x},t) = \frac{1}{2}\int_{\mathbf{y}} E(\mathbf{x},\mathbf{y},t)S_0\mathbf{y}\mathbf{y}^T d\mathbf{y}. \tag{A.13}$$

This is the stress that would be produced by bond distribution E for bonds that had stiffness S_0 and rest length zero. Recalling the definition of z_{b} from Equation A.1, we note that

$$\frac{\mathrm{Tr}(\underline{\underline{\sigma}}_0^{\mathrm{b}}(\mathbf{x},\mathrm{t}))}{z_{\mathrm{b}}(\mathbf{x},t)} = \frac{\frac{1}{2}\int_{\mathbf{y}} E(\mathbf{x},\mathbf{y},t)S_0|\mathbf{y}|^2 d\mathbf{y}}{\int_{\mathbf{y}} E(\mathbf{x},\mathbf{y},t)d\mathbf{y}} = \frac{S_0}{2} < |\mathbf{y}|^2 > (\mathbf{x},t).$$

Hence,

$$< |\mathbf{y}|^2 > (\mathbf{x},t) = \frac{2}{S_0}\frac{\mathrm{Tr}(\underline{\underline{\sigma}}_0^{\mathrm{b}}(\mathbf{x},\mathrm{t}))}{z_{\mathrm{b}}(\mathbf{x},t)} \tag{A.14}$$

is the local mean-squared bond length at location $\mathbf{x}$. From this equation, we see that an approximation to $< |\mathbf{y}| > (\mathbf{x},t)$ is

$$< |\mathbf{y}| > (\mathbf{x},t) \approx \sqrt{\frac{2}{S_0}\frac{\mathrm{Tr}(\underline{\underline{\sigma}}_0^{\mathrm{b}}(\mathbf{x},\mathrm{t}))}{z_{\mathrm{b}}(\mathbf{x},t)}}. \tag{A.15}$$

Returning to the case that $S(|\mathbf{y}|) = S_0(1 - \frac{R}{|\mathbf{y}|})$, we see from Equation A.2, that

$$\underline{\underline{\sigma}}^{\mathrm{b}}(\mathbf{x},t) = \tfrac{1}{2}\int_{\mathbf{y}} E(\mathbf{x},\mathbf{y},t)S_0\mathbf{y}\mathbf{y}^T d\mathbf{y} - \tfrac{1}{2}\int_{\mathbf{y}} E(\mathbf{x},\mathbf{y},t)S_0\tfrac{R}{|\mathbf{y}|}\mathbf{y}\mathbf{y}^T d\mathbf{y}. \tag{A.16}$$

The first integral is $\underline{\underline{\sigma}}^{\mathrm{b}}_0$ and the second integral can be approximated by

$$\tfrac{1}{2}\int_{\mathbf{y}} E(\mathbf{x},\mathbf{y},t)S_0\tfrac{R}{|\mathbf{y}|}\mathbf{y}\mathbf{y}^T d\mathbf{y} \approx \tfrac{R}{<|\mathbf{y}|>}\tfrac{1}{2}\int_{\mathbf{y}} E(\mathbf{x},\mathbf{y},t)S_0\mathbf{y}\mathbf{y}^T d\mathbf{y} = \tfrac{R}{<|\mathbf{y}|>}\underline{\underline{\sigma}}^{\mathrm{b}}_0,$$

where $< |\mathbf{y}| >$ is itself estimated using Eq. A.15. For this article, we *define* $\underline{\underline{\sigma}}^{\mathrm{b}}$ by the formula

$$\underline{\underline{\sigma}}^{\mathrm{b}}(\mathbf{x},t) = \left(1 - \sqrt{\frac{2}{S_0}\frac{\mathrm{Tr}(\underline{\underline{\sigma}}^{\mathrm{b}}_0(\mathbf{x},\mathrm{t}))}{z_{\mathrm{b}}(\mathbf{x},t)}}\right)\underline{\underline{\sigma}}^{\mathrm{b}}_0(\mathbf{x},t). \tag{A.17}$$

Hence, to evaluate $\underline{\underline{\sigma}}^{\mathrm{b}}(\mathbf{x},t)$, it suffices to know $\underline{\underline{\sigma}}^{\mathrm{b}}_0(\mathbf{x},t)$ and $z_{\mathrm{b}}(\mathbf{x},t)$. We next derive evolution equations for $\underline{\underline{\sigma}}^{\mathrm{b}}_0$ and z_{b}. From the definition of $\underline{\underline{\sigma}}^{\mathrm{b}}_0(\mathbf{x},t)$ and Eq. A.12, we see that

$$\begin{aligned}\frac{\partial \underline{\underline{\sigma}}^{\mathrm{b}}_0}{\partial t} = {} & \underbrace{\tfrac{1}{2}\int_{\mathbf{y}}\left(\alpha^{coh}_{aa}(|\mathbf{y}|)\phi_{\mathrm{a}}(\mathbf{x},t)^2 + 2\alpha^{coh}_{ab}(|\mathbf{y}|)\phi_{\mathrm{a}}(\mathbf{x},t)\phi_{\mathrm{b}}(\mathbf{x},t) + \alpha^{coh}_{bb}(|\mathbf{y}|)\phi_{\mathrm{b}}(\mathbf{x},t)^2\right)S(|\mathbf{y}|)\mathbf{y}\mathbf{y}^T d\mathbf{y}}_{(A)} \\ & - \underbrace{\tfrac{1}{2}\int_{\mathbf{y}}\beta(|\mathbf{y}|)ES(|\mathbf{y}|)\mathbf{y}\mathbf{y}^T d\mathbf{y}}_{(B)} - \underbrace{\tfrac{1}{2}\int_{\mathbf{y}}\nabla_x\cdot(E\,\mathbf{u}_{\mathrm{b}})S(|\mathbf{y}|)\mathbf{y}\mathbf{y}^T d\mathbf{y}}_{(C)} - \underbrace{\tfrac{1}{2}\int_{\mathbf{y}}\Big[(\mathbf{y}\cdot\nabla\mathbf{u}_{\mathrm{b}})\cdot\nabla_y E\Big]S(|\mathbf{y}|)\mathbf{y}\mathbf{y}^T d\mathbf{y}}_{(D)} \\ & - \underbrace{\tfrac{1}{2}\int_{\mathbf{y}}E\,(\nabla_x\cdot\mathbf{u}_{\mathrm{b}})S(|\mathbf{y}|)\mathbf{y}\mathbf{y}^T d\mathbf{y}}_{(E)}.\end{aligned} \tag{A.18}$$

Several of the labelled terms simplify immediately:

$$\begin{aligned}(A) = {} & {\phi_{\mathrm{a}}}^2(\mathbf{x},t)\Big(\tfrac{1}{6}\int_{\mathbf{y}}\alpha^{coh}_{aa}(|\mathbf{y}|)S_0|\mathbf{y}|^2 d\mathbf{y}\Big)\underline{\underline{I}} \\ & + 2\phi_{\mathrm{a}}(\mathbf{x},t)\phi_{\mathrm{b}}(\mathbf{x},t)\Big(\tfrac{1}{6}\int_{\mathbf{y}}\alpha^{coh}_{ab}(|\mathbf{y}|)S_0|\mathbf{y}|^2 d\mathbf{y}\Big)\underline{\underline{I}} \\ & + {\phi_{\mathrm{b}}}^2(\mathbf{x},t)\Big(\tfrac{1}{6}\int_{\mathbf{y}}\alpha^{coh}_{bb}(|\mathbf{y}|)S_0|\mathbf{y}|^2 d\mathbf{y}\Big)\underline{\underline{I}}, \\ (C) = {} & \nabla\cdot(\mathbf{u}_{\mathrm{b}}\underline{\underline{\sigma}}^{\mathrm{b}}_0), \\ (E) = {} & \underline{\underline{\sigma}}^{\mathrm{b}}_0(\mathbf{x},t)\nabla\cdot\mathbf{u}_{\mathrm{b}}(\mathbf{x},t).\end{aligned}$$

For term (B), we use the approximate closure we introduced in Fogelson & Guy (2004), in which $\beta(|\mathbf{y}|)$ is replaced by a function of the average local bond length, and so

$$(B) \approx \beta(< |\mathbf{y}| >^2)\underline{\underline{\sigma}}^{\mathrm{b}}_0,$$

where the β in this equation is generally different from, but related to, the β in the original expression for term (B) (Guy, 2004a; Guy, 2004b).

Toward simplifying term (D), look at the ij entry of the expression defining (D) and do integration by parts to find

$$(D)_{ij} = \tfrac{1}{2}\int_{\mathbf{y}}\Big[\sum_k\Big(\sum_l y_l\frac{\partial u_k}{\partial x_l}\frac{\partial E}{\partial y_k}\Big)\Big]S(|\mathbf{y}|)y_iy_jd\mathbf{y} = -\tfrac{1}{2}\sum_k\sum_l\frac{\partial u_k}{\partial x_l}\int_{\mathbf{y}}E\frac{\partial}{\partial y_k}\Big(S(|\mathbf{y}|)y_ly_iy_j\Big)d\mathbf{y}.$$

Using the product rule and noting that, because we are assuming $S(|\mathbf{y}|) = S_0$ is constant, $\frac{\partial}{\partial y_k}S(|\mathbf{y}|) = 0$, we obtain

$$\begin{aligned}
D_{ij} &= -\tfrac{1}{2}\sum_k\sum_l\frac{\partial u_k}{\partial x_l}\int_{\mathbf{y}}ES_0y_iy_j\delta_{kl}d\mathbf{y} - \tfrac{1}{2}\sum_k\sum_l\frac{\partial u_k}{\partial x_l}\int_{\mathbf{y}}ES_0y_ly_j\delta_{ik}d\mathbf{y} - \tfrac{1}{2}\sum_k\sum_l\frac{\partial u_k}{\partial x_l}\int_{\mathbf{y}}ES_0y_ly_i\delta_{jk}d\mathbf{y}\\
&= -\sum_k\frac{\partial u_k}{\partial x_k}\Big(\tfrac{1}{2}\int_{\mathbf{y}}ES_0y_iy_jd\mathbf{y}\Big) - \sum_l\frac{\partial u_i}{\partial x_l}\Big(\tfrac{1}{2}\int_{\mathbf{y}}ES_0y_ly_jd\mathbf{y}\Big) - \sum_l\frac{\partial u_j}{\partial x_l}\Big(\tfrac{1}{2}\int_{\mathbf{y}}ES_0y_ly_id\mathbf{y}\Big)\\
&= -(\nabla\cdot\mathbf{u}_{\mathrm{b}})\underline{\underline{\sigma}}^{\mathrm{b}}_{0ij} - (\underline{\underline{\sigma}}^{\mathrm{b}}_0\nabla\mathbf{u}_{\mathrm{b}})_{ji} - (\underline{\underline{\sigma}}^{\mathrm{b}}_0\nabla\mathbf{u}_{\mathrm{b}})_{ij},
\end{aligned}$$

where $(\nabla\mathbf{u}_{\mathrm{b}})_{mn} = \frac{\partial(u_b)_n}{\partial x_m}$. Hence,

$$(D) = -(\nabla\cdot\mathbf{u}_{\mathrm{b}})\underline{\underline{\sigma}}^{\mathrm{b}}_0 - (\underline{\underline{\sigma}}^{\mathrm{b}}_0\nabla\mathbf{u}_{\mathrm{b}}) - (\underline{\underline{\sigma}}^{\mathrm{b}}_0\nabla\mathbf{u}_{\mathrm{b}})^T.$$

Using the expressions for the various terms in Eq. A.18, we obtain

$$\begin{aligned}
\frac{\partial\underline{\underline{\sigma}}^{\mathrm{b}}_0}{\partial t} = &\underbrace{\Big(\phi_{\mathrm{a}}(\mathbf{x},t)^2\tfrac{1}{6}\int_{\mathbf{y}}\alpha^{coh}_{aa}(|\mathbf{y}|)S_0|\mathbf{y}|^2d\mathbf{y} + 2\phi_{\mathrm{a}}(\mathbf{x},t)\phi_{\mathrm{b}}(\mathbf{x},t)\tfrac{1}{6}\int_{\mathbf{y}}\alpha^{coh}_{ab}(|\mathbf{y}|)S_0|\mathbf{y}|^2d\mathbf{y} + \phi_{\mathrm{b}}(\mathbf{x},t)^2\tfrac{1}{6}\int_{\mathbf{y}}\alpha^{coh}_{bb}(|\mathbf{y}|)S_0|\mathbf{y}|^2d\mathbf{y}\Big)\underline{\underline{I}}}_{(A)}\\
&\underbrace{-\beta(< |\mathbf{y}|^2 >)\underline{\underline{\sigma}}^{\mathrm{b}}_0}_{(B)} \underbrace{-\nabla_x\cdot(\mathbf{u}_{\mathrm{b}}\underline{\underline{\sigma}}^{\mathrm{b}}_0)}_{(C)} + \underbrace{(\nabla\cdot\mathbf{u}_{\mathrm{b}})\underline{\underline{\sigma}}^{\mathrm{b}}_0 + (\underline{\underline{\sigma}}^{\mathrm{b}}_0\nabla\mathbf{u}_{\mathrm{b}}) + (\underline{\underline{\sigma}}^{\mathrm{b}}_0\nabla\mathbf{u}_{\mathrm{b}})^T}_{(D)} \underbrace{-\underline{\underline{\sigma}}^{\mathrm{b}}_0\nabla\cdot\mathbf{u}_{\mathrm{b}}}_{(E)}.
\end{aligned}$$

Noting that $\underline{\underline{\sigma}}^{\mathrm{b}}_0\nabla\cdot\mathbf{u}_{\mathrm{b}}$ in (E) cancels that in (D), we obtain the equation

$$\begin{aligned}
\frac{\partial\underline{\underline{\sigma}}^{\mathrm{b}}_0}{\partial t} + \nabla_x\cdot(\mathbf{u}_{\mathrm{b}}\underline{\underline{\sigma}}^{\mathrm{b}}_0) = &(\underline{\underline{\sigma}}^{\mathrm{b}}_0\nabla\mathbf{u}_{\mathrm{b}}) + (\underline{\underline{\sigma}}^{\mathrm{b}}_0\nabla\mathbf{u}_{\mathrm{b}})^T + \Big(\phi_{\mathrm{a}}(\mathbf{x},t)^2\tfrac{1}{6}\int_{\mathbf{y}}\alpha^{coh}_{aa}(|\mathbf{y}|)S_0|\mathbf{y}|^2d\mathbf{y}\\
&+ 2\phi_{\mathrm{a}}(\mathbf{x},t)\phi_{\mathrm{b}}(\mathbf{x},t)\tfrac{1}{6}\int_{\mathbf{y}}\alpha^{coh}_{ab}(|\mathbf{y}|)S_0|\mathbf{y}|^2d\mathbf{y} + \phi_{\mathrm{b}}(\mathbf{x},t)^2\tfrac{1}{6}\int_{\mathbf{y}}\alpha^{coh}_{bb}(|\mathbf{y}|)S_0|\mathbf{y}|^2d\mathbf{y}\Big)\underline{\underline{I}}\\
&- \beta(< |\mathbf{y}|^2 >)\underline{\underline{\sigma}}^{\mathrm{b}}_0.
\end{aligned} \tag{A.19}$$

Now, we derive the partial differential equation for z_b. From the definition of z_b (Eq. A.1), the equation for E (Eq. A.12), and the closure approximation for the bond breaking rate, it follows that

$$\frac{\partial z_b}{\partial t} = -\nabla_x \cdot (\mathbf{u}_b z_b) - \int_{\mathbf{y}} (\mathbf{y} \cdot \nabla \mathbf{u}_b) \cdot \nabla_y E d\mathbf{y} - z_b \nabla \cdot \mathbf{u}_b + \phi_a(\mathbf{x},t)^2 \int_{\mathbf{y}} \alpha_{aa}^{coh}(|\mathbf{y}|) d\mathbf{y} \tag{A.20}$$
$$+ 2\phi_a(\mathbf{x},t)\phi_b(\mathbf{x},t) \int_{\mathbf{y}} \alpha_{ab}^{coh}(|\mathbf{y}|) d\mathbf{y} + \phi_b(\mathbf{x},t)^2 \int_{\mathbf{y}} \alpha_{bb}^{coh}(|\mathbf{y}|) d\mathbf{y} - \beta(< |\mathbf{y}|^2 >) z_b.$$

Note that

$$\int_{\mathbf{y}} (\mathbf{y} \cdot \nabla \mathbf{u}_b) \cdot \nabla_y E d\mathbf{y} = -\int_{\mathbf{y}} E \nabla_y \cdot (\mathbf{y} \cdot \nabla \mathbf{u}_b) d\mathbf{y} = -\int_{\mathbf{y}} E \sum_k \frac{\partial}{\partial y_k} (\sum_l y_l \frac{\partial u_k}{\partial x_l}) d\mathbf{y}$$
$$= -\sum_k \sum_l \int_{\mathbf{y}} E \delta_{kl} \frac{\partial u_k}{\partial x_l} d\mathbf{y} = -z_b \nabla \cdot \mathbf{u}_b.$$

Using this in Equation A.20 yields

$$\frac{\partial z_b}{\partial t} + \nabla_x \cdot (\mathbf{u}_b z_b) = \phi_a(\mathbf{x},t)^2 \int_{\mathbf{y}} \alpha_{aa}^{coh}(|\mathbf{y}|) d\mathbf{y} + 2\phi_a(\mathbf{x},t)\phi_b(\mathbf{x},t) \int_{\mathbf{y}} \alpha_{ab}^{coh}(|\mathbf{y}|) d\mathbf{y} \tag{A.21}$$
$$+ \phi_b(\mathbf{x},t)^2 \int_{\mathbf{y}} \alpha_{bb}^{coh}(|\mathbf{y}|) d\mathbf{y} - \beta(< |\mathbf{y}|^2 >) z_b.$$

We define K_{aa}^{coh}, K_{ab}^{coh}, and K_{bb}^{coh} by

$$K_{aa}^{coh}(n_b^{\max})^2 = \int_{\mathbf{y}} \alpha_{aa}^{coh}(|\mathbf{y}|) d\mathbf{y}, \qquad K_{ab}^{coh}(n_b^{\max})^2 = 2\int_{\mathbf{y}} \alpha_{ab}^{coh}(|\mathbf{y}|) d\mathbf{y}, \qquad K_{bb}^{coh}(n_b^{\max})^2 = \int_{\mathbf{y}} \alpha_{bb}^{coh}(|\mathbf{y}|) d\mathbf{y}$$

and we assume that the ratios $\frac{\int \alpha_{ij}^{coh} |\mathbf{y}|^2 d\mathbf{y}}{\int \alpha_{ij}^{coh} d\mathbf{y}}$ are equal for $ij = aa,\ ab,\ and\ bb$. We define C_1 by

$$C_1 = \frac{S_0}{6} \frac{\int \alpha_{ij}^{coh}(|\mathbf{y}|) |\mathbf{y}|^2 d\mathbf{y}}{\int \alpha_{ij}^{coh}(|\mathbf{y}|) d\mathbf{y}}, \tag{A.22}$$

and note that

$$C_1 K_{aa}^{coh}(n_b^{\max})^2 = \tfrac{1}{6} \int \alpha_{aa}^{coh}(|\mathbf{y}|) S_0 |\mathbf{y}|^2 d\mathbf{y},$$
$$C_1 K_{ab}^{coh}(n_b^{\max})^2 = \tfrac{1}{3} \int \alpha_{ab}^{coh}(|\mathbf{y}|) S_0 |\mathbf{y}|^2 d\mathbf{y},$$
$$C_1 K_{bb}^{coh}(n_b^{\max})^2 = \tfrac{1}{6} \int \alpha_{bb}^{coh}(|\mathbf{y}|) S_0 |\mathbf{y}|^2 d\mathbf{y}.$$

Then,

$$\frac{\partial \underline{\underline{\sigma}}_0^{\mathrm{b}}}{\partial t} + \nabla \cdot (\mathbf{u}_{\mathrm{b}} \underline{\underline{\sigma}}_0^{\mathrm{b}}) = \left(\underline{\underline{\sigma}}_0^{\mathrm{b}} \nabla \mathbf{u}_{\mathrm{b}}\right) + \left(\underline{\underline{\sigma}}_0^{\mathrm{b}} \nabla \mathbf{u}_{\mathrm{b}}\right)^T + C_1 \alpha(\phi_{\mathrm{a}}(\mathbf{x}, t), \phi_{\mathrm{b}}(\mathbf{x}, t)) \underline{\underline{I}} - \beta(< |\mathbf{y}|^2 >) \underline{\underline{\sigma}}_0^{\mathrm{b}}, \tag{A.23}$$

$$\frac{\partial z_{\mathrm{b}}}{\partial t} + \nabla \cdot (\mathbf{u}_{\mathrm{b}} z_{\mathrm{b}}) = \alpha(\phi_{\mathrm{a}}(\mathbf{x}, t), \phi_{\mathrm{b}}(\mathbf{x}, t)) - \beta(< |\mathbf{y}|^2 >) z_{\mathrm{b}}, \tag{A.24}$$

where

$$\alpha(\phi_{\mathrm{a}}, \phi_{\mathrm{b}}) = K_{aa}^{coh} (n_{\mathrm{b}}^{\max})^2 {\phi_{\mathrm{a}}}^2 + K_{ab}^{coh} (n_{\mathrm{b}}^{\max})^2 \phi_{\mathrm{a}} \phi_{\mathrm{b}} + K_{bb}^{coh} (n_{\mathrm{b}}^{\max})^2 {\phi_{\mathrm{b}}}^2. \tag{A.25}$$

Equations A.23 and A.24 differ from those in our single phase model in that the advective term is in divergence form and the bond and stress formation terms are more complex. The derivations of Equations A.23 and A.24 have ignored the saturation of binding sites on bound platelets. To account for this, the $n_{\mathrm{b}}^{\max} \phi_{\mathrm{b}}$ terms in these equations are replaced by the function η as defined in section 2.4 which gives the average number of unoccupied binding sites within a prescribed small distance of $\mathbf{x}$.